Tangled gene-for-gene interactions mediate co-evolution of the rice NLR immune receptor Pik and blast fungus effector proteins

Yu Sugihara[1,2,3], Yoshiko Abe[1], Hiroki Takagi[1,#a], Akira Abe[1], Motoki Shimizu[1], Kazue Ito[1], Eiko Kanzaki[1], Kaori Oikawa[1], Jiorgos Kourelis[3], Thorsten Langner[3], Joe Win[3], Aleksandra Białas[3], Daniel Lüdke[3], Izumi Chuma[4], Hiromasa Saitoh[1,#b], Michie Kobayashi[1,#c], Shuan Zheng[1,2], Yukio Tosa[5], Mark J. Banfield[6], Sophien Kamoun[3]*, Ryohei Terauchi[1,2]*, Koki Fujisaki[1]*

[1] Iwate Biotechnology Research Center, Kitakami, Iwate, 024-0003, Japan
[2] Crop Evolution Laboratory, Kyoto University, Mozume, Muko, Kyoto, 617-0001, Japan
[3] The Sainsbury Laboratory, University of East Anglia, Norwich, NR4 7UH, United Kingdom
[4] Obihiro University of Agriculture and Veterinary Medicine, Obihiro, 080-8555, Japan
[5] Graduate School of Agricultural Science, Kobe University, Kobe, 657-8501, Japan
[6] Department of Biochemistry and Metabolism, John Innes Centre, Norwich Research Park, Norwich, NR4 7UH, United Kingdom
[#a] Current Address: Faculty of Bioresources and Environmental Sciences, Ishikawa Prefectural University, Nonoichi 921-8836, Japan
[#b] Current Address: Department of Molecular Microbiology, Tokyo University of Agriculture, Setagaya-ku, Tokyo 156-8502, Japan
[#c] Current Address: Institute of Agrobiological Sciences, National Agriculture and Food Research Organization (NARO), Kannondai 2-1-2, Tsukuba, Ibaraki 305-8602, Japan

*Corresponding authors
E-mail: sophien.kamoun@tsl.ac.uk (SK); terauchi@ibrc.or.jp (RT); k-fujisaki@ibrc.or.jp (KF)

Abstract

Studies focused solely on single organisms can fail to identify the networks underlying host–pathogen gene-for-gene interactions. Here, we integrate genetic analyses of rice (*Oryza sativa*, host) and rice blast fungus (*Magnaporthe oryzae*, pathogen) and uncover a new pathogen recognition specificity of the rice nucleotide-binding domain and leucine-rich repeat protein (NLR) immune receptor Pik, which mediates resistance to *M. oryzae* expressing the avirulence effector gene *AVR-Pik*. Rice Piks-1, encoded by an allele of *Pik-1*, recognizes a previously unidentified effector encoded by the *M. oryzae* avirulence gene *AVR-Mgk1*, which is found on a mini-chromosome. *AVR-Mgk1* has no sequence similarity to known *AVR-Pik* effectors, and is prone to deletion from the mini-chromosome mediated by repeated *Inago2* retrotransposon sequences. AVR-Mgk1 is detected by Piks-1 and by other Pik-1 alleles known to recognize AVR-Pik effectors; recognition is mediated by AVR-Mgk1 binding to the integrated heavy metal-associated domain of Piks-1 and other Pik-

1 alleles. Our findings highlight how complex gene-for-gene interaction networks can be disentangled by applying forward genetics approaches simultaneously to the host and pathogen. We demonstrate dynamic co-evolution between an NLR integrated domain and multiple families of effector proteins.

Introduction

Immune recognition between plant hosts and pathogens is often mediated by gene-for-gene interactions [1]. In this classical genetic model, a match between a single plant disease resistance (*R*) gene and a single pathogen avirulence effector (*AVR*) gene leads to pathogen recognition and induces plant immunity [1]. This model is the foundation for understanding *R–AVR* interactions, leading to molecular cloning of numerous *R* and *AVR* genes. However, recent studies revealed there can be a higher level of complexity that expanded the gene-for-gene model [2–5]. In a given plant–pathogen combination, immune recognition frequently involves multiple tangled *R–AVR* interactions. In this case, knockout or knock-in of single host or pathogen genes does not alter the phenotype, hampering attempts to identify genes involved in the interaction. To overcome this problem, we need host and pathogen lines that allow dissection of a single of *R–AVR* interactions. Lines containing only a single *R* or *AVR* locus can be selected from recombinant lines derived from a cross between genetically distant parents. Such materials have been used to analyse the host or pathogen, but have not been simultaneously applied to both the host and pathogen. In this study, we employed integrated genetics approaches on the host and pathogen to unravel complex interactions between rice (*Oryza sativa*) and the rice blast fungus *Magnaporthe oryzae* (syn. *Pyricularia oryzae*).

Studies on the *M. oryzae*–host pathosystem benefited from examining gene-for-gene interactions. The filamentous ascomycete fungus *M. oryzae* causes blast disease in cereal crops, such as rice, wheat (*Triticum aestivum*), and foxtail millet (*Setaria italica*) [6,7]. *M. oryzae* consists of genetic subgroups that have infection specificities for particular host genera [7]. This host specificity is often determined by a repertoire of lineage-specific genes [8–11]. The gain and loss of these lineage-specific genes sometimes results in host jump and specialization [10,11]. Therefore, identifying host *R* genes with corresponding pathogen *AVR* genes is crucial to understanding host specificities.

Pathogen effectors modulate host cell physiology to promote susceptibility [12]. In *M. oryzae*, at least 15 effector genes have been identified as *AVR* genes [11,13–25]. The protein structures of AVR-Pik, AVR-Pia, AVR1-CO39, AvrPiz-t, AvrPib, and AVR-Pii have been experimentally determined [26–30]. All of their protein structures, except for the zinc-finger fold of AVR-Pii [30], share a similar six-stranded β-sandwich structure called the MAX (*Magnaporthe* Avrs and ToxB-like) fold [27,31]. This sequence-unrelated MAX effector superfamily has expanded in *M. oryzae* and *M. grisea*, probably through diversifying selection and adaptation to the host environment [27,32,33]. Recent advances in protein structure prediction enabled secretome-wide structure prediction to annotate MAX effectors and other effector families in *M. oryzae*

[33,34]. Nonetheless, most MAX effectors remain functionally uncharacterized, including their ability to activate plant immunity.

Similar to other plant pathogenic fungi [35–40], some *M. oryzae* strains contain supernumerary chromosomes called mini-chromosomes (syn. B-, accessory-, or conditionally dispensable chromosomes) in addition to the essential core chromosomes [41–43]. *M. oryzae* mini-chromosomes are smaller than core chromosomes, are rich in transposable elements, and have a lower gene density [44,45]. *M. oryzae* mini-chromosomes can be hypervariable with frequent inter-chromosomal translocations between core chromosomes and mini-chromosomes [45,46]. Since mini-chromosomes often carry virulence-related genes, such as *AVR-Pita* [15,46], *AVR-Pik* [17,45,47,48], a polyketide synthase *Avirulence Conferring Enzyme 1* (*ACE1*) [45,49], *PWL2* [14,44], *Biotrophy-associated secreted1* (*BAS1*) [44,50], and *AvrPib* [22,44], they are thought to contribute to host adaptation, although the precise mechanisms remain unclear [44–48,51].

To detect invading pathogens, plants evolved disease-resistance genes [52]. Nucleotide-binding domain and leucine-rich repeat protein (NLR) receptors constitute the predominant class of plant intracellular *R* genes [52–54]. The typical domain architecture of plant NLRs is characterized by the central NB-ARC (nucleotide-binding adaptor shared by Apaf-1, certain *R* genes and CED-4) domain and the C-terminal leucine-rich repeat (LRR) domain [55]. The N-terminus contains a TIR (Toll/interleukin 1 receptor), CC (Rx-type coiled-coil), or CC_R (RPW8-type CC) domain [56–58]. NLR genes are often clustered [59], and may consist of a genetically linked pair of NLRs in head-to-head orientation [60–64]. In the prevailing model, NLR pairs consist of functionally specialized sensor and helper NLRs [2,53,64]. Sensor NLRs directly or indirectly recognize pathogen effectors, while helper NLRs are required by sensor NLRs to activate defence signalling. Some sensor NLRs contain non-canonical integrated domains that act as baits for pathogen effectors [65,66].

In rice, three CC-type NLR pairs, *Pik* (Pik-1/Pik-2), *Pia* (Pia-2/Pia-1, also known as RGA5/RGA4), and *Pii* (Pii-2/Pii-1), have been characterized [60,63,67]. These NLR pairs are genetically linked in head-to-head orientation, and their sensor NLRs (Pik-1, Pia-2, and Pii-2, respectively) have non-canonical integrated domains that mediate pathogen detection. Pik-1 and Pia-2 have a heavy metal-associated (HMA, also known as RATX) domain as the integrated domain [28,63,68]. For Pik-1, the integrated HMA domain, located between the CC and NB-ARC domains, directly binds the *M. oryzae* effectors AVR-PikD, E, and A, and this binding is required to trigger the immune response [28,69–72]. By contrast, the Pia-2 integrated HMA domain C-terminal to the LRR [63] directly binds the two *M. oryzae* effectors AVR-Pia and AVR1-CO39, which have unrelated sequences [68,73,74]. AVR-Pik and AVR-Pik like (APikL) proteins bind members of the host HMA domain family, called small HMA (sHMA) proteins, which may act as susceptibility factors during pathogen infection [32,75–77]. Therefore, the HMA domains of Pik-1 and Pia-2 are considered to act as baits to trap pathogen effectors [65,66]. Lastly, Pii-2 has an integrated nitrate (NO_3)-induced (NOI) domain after the LRR domain [78]. Pii-2 indirectly recognizes the *M. oryzae* effector AVR-Pii via a complex between rice EXO70 (a subunit of the exocyst complex) and the NOI domain of Pii-2 [30,78,79]. The

integrated domains of these rice sensor NLRs have been used for protein engineering to confer broad-spectrum resistance [80–85].

Since cloning of the NLR pair *Pikm* [60], at least five additional *Pik* alleles (*Pikp*, *Pik**, *Pikh*, *Pike*, and *Piks*) have been identified at the *Pik* locus [60,86–91]. This allelic diversification is likely driven by an arms race co-evolution with *M. oryzae AVR-Pik* effectors, where a few Pik amino acid polymorphisms often define their recognition specificity [69–72,92]. The *Pik* alleles, except for *Piks*, were genetically defined as producing resistance against specific isolates of the blast fungus [60,87–91]. However, no report is available for *Piks*-conferred resistance and its target *AVR* gene [92].

In this study, we aimed to uncover additional functions of the well-studied rice Pik immune receptors by integrating host and pathogen genetic analyses (**Fig. 1**). This revealed a previously overlooked interaction between a Pik receptor and a *M. oryzae* effector. We found that Piks-1 detects the *M. oryzae* effector AVR-Mgk1, which is unrelated to the AVR-Pik family in sequence and is encoded on a *M. oryzae* mini-chromosome. The integrated HMA domain of Piks-1 binds AVR-Mgk1 but not AVR-PikD, whereas the HMA domains of other Pik-1 alleles bind AVR-PikD and AVR-Mgk1. This study illustrates the potential of integrated host and pathogen genetic analyses to unravel complex gene-for-gene interactions.

Results

Piks contributes to resistance against *M. oryzae* isolate O23

The *japonica*-type rice cultivar Hitomebore is resistant to the *M. oryzae* isolates TH3o and O23, which originate from Thailand and Indonesia, respectively (**Fig. 2A**). In contrast, the *japonica*-type rice cultivar Moukoto is susceptible to these isolates (**Fig. 2A**). To determine the loci contributing to the resistance of Hitomebore against TH3o and O23, we produced rice recombinant inbred lines (RILs) derived from a cross between Hitomebore and Moukoto, resulting in 249 RILs that were subsequently subjected to whole-genome sequencing (**Table S1**). We used 156,503 single nucleotide polymorphism (SNP) markers, designed from the parental genomes, for genetic association analysis on 226 RILs (**Table S2**). This analysis identified a locus strongly associated with resistance to TH3o on chromosome 1 (**Fig. 2B**), and loci associated with resistance to O23 on chromosomes 1 and 11 (**Fig. 2C**). The chromosome 1 locus, associated with resistance to both TH3o and O23, contained the NLR gene *Pish*, which confers moderate resistance to *M. oryzae* [93]. In contrast, the locus on chromosome 11 was associated with resistance to O23 only (**Fig. 2C**), and contained the NLR gene *Piks*, an allele of *Pik*. A subset of the RILs, including RIL #58, contained the Moukoto-type *Pish* allele and the Hitomebore-type *Piks* allele and was susceptible to TH3o but resistant to O23 (**Fig. 2A**), suggesting the role of *Piks* in resistance against O23.

153 All known *Pik* alleles function as paired NLR genes, consisting of *Pik-1* (sensor NLR) and *Pik-2* (helper
154 NLR), which cooperate to trigger an immune response [60,94]. Therefore, we performed RNA interference
155 (RNAi)-mediated knockdown of *Piks-1* and *Piks-2* in the RIL #58 (*Pish* -, *Piks* +) background to test their
156 roles in resistance to O23. For both *Piks-1* and *Piks-2*, we targeted two different regions of the open reading
157 frame (**Fig. S1**) and isolated two independent lines per RNAi construct. We used reverse transcription
158 quantitative PCR (RT-qPCR) to analyse *Piks-1* and *Piks-2* expression in these lines (**Fig. S2**). Subsequently,
159 we inoculated the RNAi lines and RIL #58 as a control with the TH3o and O23 isolates (**Fig. 2D**). The *Piks-*
160 *1* and *Piks-2* knockdown lines were susceptible to O23, indicating that *Piks* is involved in resistance to O23.
161
162 Although *Pik* is a well-studied NLR gene, the *Piks* allele has not been functionally characterized. Therefore,
163 we investigated the evolutionary relationship of *Piks* and other *Pik* alleles by reconstructing a phylogenetic
164 tree focusing on the *Pik-1* sensor NLRs (**Fig. 3A**), which showed that *Piks-1* is most closely related to *Pikm-*
165 *1*. Comparing amino acid sequences between Piks and Pikm revealed only two amino acid replacements.
166 These two residues were located in the HMA domain of Pik-1 (**Fig. 3B**). The HMA domain of Pikm (Pikm-
167 HMA) was crystalized in complex with the *M. oryzae* effector protein AVR-PikD [70]; the two amino acids
168 differentiating Piks-HMA from Pikm-HMA were located at the interface of Pikm-HMA and AVR-PikD (**Fig.**
169 **3C**), suggesting that these amino acid replacements may affect Pik-1 binding to the AVR-Pik effector.
170 Amino acid sequences of the helper NLRs, Piks-2 and Pikm-2, were identical (**Fig. 3B**).
171
172 ***Magnaporthe* genetics reveals an avirulence effector gene *AVR-Mgk1* encoded on a mini-chromosome**
173
174 To identify the *AVR* gene of *M. oryzae* isolate O23 that encodes the effector recognized by Piks, we crossed
175 TH3o and O23 (**Fig. 1** and **4A**). We first assembled the genome sequence of O23 into 11 contigs with a total
176 size of 43 Mbp using long sequence reads from Oxford Nanopore Technologies (**Table S3**). The
177 Benchmarking Universal Single-Copy Orthologs (BUSCOs) value of the assembled genome [95] was 98.2%
178 for the complete BUSCOs using the *Sordariomyceta* odb9 dataset (**Table S3**). Comparing the O23 assembled
179 contigs with the reference genome version MG8 of *M. oryzae* isolate 70-15 [96] by dot plot analysis revealed
180 that the O23 genome was assembled almost completely end-to-end (**Fig. S3**). Compared to *M. oryzae* isolate
181 70-15, the O23 genome contained a large rearrangement between chromosome 1 and 6, which has been
182 reported in other *M. oryzae* isolates [44,97–99].
183
184 A study using contour-clamped homogeneous electric field (CHEF) gel electrophoresis identified a mini-
185 chromosome in O23 and reconstructed the sequence of the mini-chromosome region containing the *AVR-*
186 *Pita* effector [46]. To identify the contigs corresponding to the mini-chromosome in our O23 assembly, we
187 used AVR-Pita as an anchor using the alignment tool Exonerate [100]. AVR-Pita matched the 824-kbp
188 contig named O23_contig_1, which was separately assembled from the core chromosomes (chromosomes
189 1–7). The presence of the telomeric repetitive sequence TTAGGG [101] in both ends suggested that this
190 contig is a complete mini-chromosome. AVR-Pita was located close to the telomere of the O23_contig_1 as

191 previously reported [46], suggesting that O23_contig_1 likely represents the O23 mini-chromosome [46].
192 The entire sequence of the O23_contig_1 was absent from the TH3o genome (**Fig. S4B**).
193
194 We obtained 144 F_1 progeny from a cross between TH3o and O23 and subjected them to whole-genome
195 sequencing (**Table S4**). We then compared the TH3o and O23 genome sequences and extracted 7,867 SNP
196 markers for the core chromosomes (chromosomes 1–7) and 265 presence/absence markers for other contigs,
197 including O23_contig_1. Next, we inoculated RIL #58 (*Pish* -, *Piks* +) with each of the *M. oryzae* F_1 progeny
198 and recorded the lesion size (**Table S5**). There was a strong association between lesion size and the DNA
199 marker on the mini-chromosome sequence O23_contig_1 (**Fig. 4B**). The *p*-values of the DNA markers
200 showing higher levels of association were almost constant across O23_contig_1 (**Fig. 4C**), except for
201 position 755–785 kbp with lower *p*-values. This suggested that the candidate *AVR* gene is located on this
202 mini-chromosome region.
203
204 To identify the genes expressed within the candidate region, we performed RNA sequencing (RNA-seq) of
205 O23 and TH3o inoculated on barley (*Hordeum vulgare*) cv. Nigrate. Two genes were specifically expressed
206 from the candidate region of O23. These two genes had an identical nucleotide sequence and were arranged
207 in a head-to-head orientation. We named these genes *AVR-Mgk1* (*Magnaporthe* gene recognized by *Pik*).
208 Sequences similar to *AVR-Mgk1* were not detected in the TH3o genome. These results suggest that AVR-
209 Mgk1 may encode the *M. oryzae* effector recognized by Piks.
210
211 To confirm the recognition of AVR-Mgk1 by Piks, we performed a punch inoculation assay using the *M.*
212 *oryzae* isolate Sasa2, which is compatible with all the cultivars tested in this study, transformed with *AVR-*
213 *PikD* or *AVR-Mgk1* (**Fig. 4D** and **4E** and **S5** and **S6**). Sasa2 transformants expressing *AVR-PikD* infected
214 RIL #58 (*Piks*) rice plants, but the transformants expressing *AVR-Mgk1* could not (**Fig. 4D** and **4E** and **S5**),
215 indicating that Piks recognizes AVR-Mgk1. Furthermore, Sasa2 transformants expressing *AVR-Mgk1*
216 triggered resistance in the rice cultivar Tsuyuake (*Pikm*). To investigate the recognition specificity of the
217 proteins encoded by other rice *Pik* alleles for AVR-Mgk1, we performed punch inoculation assays with K60
218 (*Pikp*) and Kanto51 (*Pik**) rice plants (**Fig. S7**). Sasa2 transformants expressing *AVR-Mgk1* were recognized
219 by K60 (*Pikp*) and Kanto51 (*Pik**), showing that the proteins encoded by *Pikm*, *Pikp*, and *Pik** also detect
220 AVR-Mgk1 (**Fig. S7**). These results indicate that AVR-Mgk1 is broadly recognized by Pik proteins.
221
222 In addition to *AVR-Mgk1*, we identified a sequence similar to *AVR-PikD* in O23_contig_1 (**Fig. 4C**). This
223 *AVR-PikD*-like gene carries a frameshift mutation, and thus encodes a protein with additional amino acids
224 at the C-terminus (**Fig. S8A**). We named it *AVR-PikD_O23*. To investigate whether Piks recognizes AVR-
225 PikD_O23, we inoculated RIL #58 (*Piks*) and Tsuyuake (*Pikm*) with Sasa2 transformants expressing *AVR-*
226 *PikD_O23* (**Fig. S8B**). The transformants expressing *AVR-PikD_O23* infected RIL #58 (*Piks*), but not
227 Tsuyuake (*Pikm*) (**Fig. S8B**), indicating that AVR-PikD_O23 is not recognized by Piks but is recognized by
228 Pikm, which is consistent with the *AVR* activity of the known *AVR-PikD* gene.

229

230 **Retrotransposon repeat sequence-mediated deletion of *AVR-Mgk1* re-establishes virulence**

231

232 The lower *p*-values of association around the *AVR-Mgk1* genes compared with the rest of the mini-
233 chromosome (**Fig. 4C**) facilitated their identification. To identify the F_1 progeny contributing to the lower
234 *p*-values, we checked the presence/absence of genetic markers on the mini-chromosome in all F_1 progeny.
235 One F_1 progeny, named d44a, lacked some markers around the *AVR-Mgk1* genes, suggesting that d44a
236 inherited the mini-chromosome sequence from O23, but lacked the *AVR-Mgk1* genes.

237

238 To elucidate the mini-chromosome structure in the d44a isolate, we sequenced the d44a genome using
239 Oxford Nanopore Technologies (**Table S3**) and compared it with the O23 genome (**Fig. 5A** and **S3**). Two
240 tandemly duplicated sequences of the retrotransposon *Inago2* flanked the *AVR-Mgk1* coding regions in O23.
241 However, in d44a, the *Inago2* sequences were directly associated without the *AVR-Mgk1* coding regions
242 (**Fig. 5A**). This suggests that an *Inago2* sequence repeat–mediated deletion of *AVR-Mgk1* occurred in d44a.
243 This deletion was approximately 30 kbp long and the sequence carrying this deletion was assembled
244 separately from the core chromosomes in d44a. This suggests that the deletion was not caused by an inter-
245 chromosome rearrangement between mini- and core chromosomes but by an intra-chromosome
246 rearrangement within or between mini-chromosomes associated with the *Inago2* sequence repeats.

247

248 To investigate the virulence of the d44a isolate in RIL #58 (*Piks*), we performed a punch inoculation assay
249 using O23 and TH3o as controls (**Fig. 5B** and **5C**). Consistent with the loss of the two *AVR-Mgk1* genes
250 from the d44a mini-chromosome (**Fig. 5A**), d44a infected RIL #58 (*Piks*) plants (**Fig. 5B** and **5C**). Since
251 d44a still carries *AVR-PikD_O23* on its mini-chromosome, this result supports that AVR-PikD_O23 is not
252 recognized by Piks.

253

254 **AVR-Mgk1 is predicted to be a MAX fold protein that belongs to a distinct family from AVR-Pik**
255 **effectors**

256

257 To determine whether AVR-Mgk1 (**Fig. 6A**) is related to the AVR-Pik effectors in amino acid sequence, we
258 performed a global alignment between AVR-Mgk1 and AVR-PikD, which revealed a sequence identity of
259 only ~10% (**Fig. S9**). Therefore, we conclude that these proteins are not related in terms of amino acid
260 sequences.

261

262 To further investigate the relationship between AVR-Mgk1 and AVR-Pik effectors, we applied TRIBE-
263 MCL clustering algorithm [102] to a dataset of putative *M. oryzae* effector proteins [31], amended with
264 AVR-Mgk1. TRIBE-MCL assigned AVR-Mgk1 and AVR-PikD (**Fig. 6B**) into different tribes. This
265 indicates that AVR-Mgk1 belongs to a distinct protein family from AVR-Pik effectors.

266

267 Although AVR-Mgk1 has little primary sequence similarity to the AVR-Pik family, AlphaFold2 [103]
268 predicted the protein structure of AVR-Mgk1 as antiparallel β sheets, characteristic of the MAX effector
269 superfamily (**Fig. 6C**) [27]. To further evaluate the structural similarity between AVR-Mgk1 and AVR-PikD,
270 we aligned the structures of AVR-Mgk1 (**Fig. 6C**) and AVR-PikD (**Fig. 6D**) in complex with the HMA
271 domain of Pikm [70] using the structure-based aligner TM-align [104]. TM-align revealed significant
272 structural similarity between the AVR-Mgk1 predicted model and AVR-PikD (**Fig. S10**) with a TM-score
273 >0.5, indicating that they share a similar fold [105]. In addition, AVR-Mgk1 contains the two cysteine
274 residues (Cys27 and Cys67, indicated by black arrowheads, **Fig. 6A**) conserved in the MAX effector
275 superfamily [27]. Overall, these results indicate that AVR-Mgk1 and AVR-PikD are MAX fold effector
276 proteins that belong to distinct families.
277
278 ***AVR-Mgk1* occurs with low frequency in *M. oryzae***
279
280 Given that Piks has a narrow recognition spectrum against *M. oryzae* [92], we investigated the distribution
281 of *AVR-Mgk1* in sequenced genomes of the blast fungus. To this end, we performed BLASTN and BLASTP
282 searches against a non-redundant NCBI database using AVR-Mgk1 sequences as query (**Table S6**). While
283 the BLASTN search failed to find any relevant hits for sequences from the non-redundant nucleotide
284 collection, the BLASTP search found one sequence in the *M. oryzae* isolate Y34 [106] with a sequence
285 identity of ~52%.
286
287 We also performed a BLASTN search against whole-genome shotgun contigs of *Magnaporthe* deposited in
288 NCBI (**Table S6**). We found sequences identical to *AVR-Mgk1* in the *M. oryzae* isolates 10100 [107] and
289 v86010 [108]. We also found two sequences with ~91% identity to *AVR-Mgk1* in *M. grisea Digitaria* isolate
290 DS9461 [109], which is a sister species of *M. oryzae* but is genetically markedly different from *M. oryzae*
291 [109,110]. These results indicate that *AVR-Mgk1* occurs with low frequency in *M. oryzae* and may derive
292 from *M. grisea*.
293
294 **The Pik-1 integrated HMA domain binds AVR-Mgk1**
295
296 The integrated HMA domains of Pia and Pik sensor NLRs (Pia-2 and Pik-1) bind multiple *M. oryzae* MAX
297 effectors [68,74,111]. Therefore, we hypothesized that AVR-Mgk1 binds the integrated HMA domain of
298 Pik-1. To investigate this, we performed yeast two-hybrid assays and *in vitro* co-immunoprecipitation (co-
299 IP) experiments (**Fig. 7A** and **7B**). The integrated HMA domain of Pikm-1 bound AVR-Mgk1 and AVR-
300 PikD, whereas the HMA domain of Piks-1 bound only AVR-Mgk1 (**Fig. 7A** and **7B**). These results indicate
301 that the Pik-1 integrated HMA domain directly binds AVR-Mgk1, and that one or both of the amino acid
302 changes in Piks-HMA hinder its binding to AVR-PikD (**Fig. 3**).
303

304 To investigate protein-protein interactions between AVR-Mgk1 and the HMA domains of other Pik proteins
305 (Pikp and Pik*), we performed yeast two-hybrid assays and *in vitro* co-IP experiments for Pikp and Pik*
306 (**Fig. S11-S15**). The integrated HMA domains of Pikp and Pik* bound AVR-Mgk1 and AVR-PikD, although
307 Pikp bound AVR-Mgk1 with a lower apparent affinity than the other Pik proteins (**Fig. S13** and **S15**). Taken
308 together, these results demonstrated that the HMA domains of all Pik proteins tested bind AVR-Mgk1, which
309 are consistent with the results of the inoculation assay (**Fig. S7**).
310
311 **Piks specifically responds to AVR-Mgk1 in a *Nicotiana benthamiana* transient expression assay**
312
313 The AVR-Pik-elicited hypersensitive response (HR) cell death mediated by Pik NLR pairs has been
314 recapitulated in *Nicotiana benthamiana* transient expression assays [28,70,94]. To investigate whether the
315 HR cell death can be recapitulated with AVR-Mgk1, we performed HR cell death assays in *N. benthamiana*
316 by transiently co-expressing *AVR-Mgk1* or *AVR-PikD* with *Piks* (*Piks-1*/*Piks-2*) or *Pikm* (*Pikm-1*/*Pikm-2*).
317 While Pikm responded to AVR-Mgk1 and AVR-PikD, Piks responded only to AVR-Mgk1 (**Fig. 7C** and
318 **7D**). AVR-Mgk1 and AVR-PikD alone did not trigger the HR in *N. benthamiana* (**Fig. S16**). These results
319 are consistent with the protein-protein interaction results (**Fig. 7A** and **7B**) and indicate that Piks has a
320 narrower effector recognition range than Pikm.
321
322 **Two polymorphisms, E229Q and A261V, between Piks and Pikm quantitatively affect the response to**
323 **AVR-Pik**
324
325 We investigated if the amino acid polymorphisms between Piks-1 and Pikm-1 (**Fig. 3**) contribute to the
326 differential response to AVR-PikD. We produced single-amino acid mutants of Piks-1 (Piks-1^{E229Q} and Piks-
327 1^{A261V}, **Fig. 8A**) and performed HR cell death assays in *N. benthamiana* by transiently co-expressing *Piks*
328 (*Piks-1*/*Piks-2*), *Piks*^{E229Q} (*Piks-1*^{E229Q}/*Piks-2*), *Piks*^{A261V} (*Piks-1*^{A261V}/*Piks-2*), or *Pikm* (*Pikm-1*/*Pikm-2*) with
329 *AVR-PikD* or *AVR-Mgk1* (**Fig. 8B-8D**). The helper NLRs Piks-2 and Pikm-2 have an identical amino acid
330 sequence (**Fig. 3B**). Both polymorphisms (E229Q and A261V) quantitatively affected the response to AVR-
331 PikD (**Fig. 8B**). Neither Piks-1^{E229Q} nor Piks-1^{A261V} achieved the same response level as Pikm; however,
332 Piks-1^{A261V} was slightly more responsive to AVR-PikD than Piks-1^{E229Q} (**Fig. 8B-8D**). The E229Q and
333 A261V mutations did not affect the response to AVR-Mgk1 (**Fig. 8C** and **8D**). These results demonstrated
334 that the Q229 and V261 residues of the HMA domain of Pikm are essential for the full response to AVR-
335 PikD.
336
337
338 **Discussion**
339
340 In this study, we revealed a gene-for-gene interaction between the well-studied rice *Pik* resistance gene and
341 *M. oryzae* effector genes. We discovered that the *Pik* allele *Piks* encodes a protein that detects the *M. oryzae*

342 effector AVR-Mgk1, a secreted protein that does not belong to the AVR-Pik effector family. Piks specifically
343 detects and responds to AVR-Mgk1, but other Pik proteins detects AVR-Mgk1 and AVR-Pik, indicating a
344 complex network of gene-for-gene interactions (**Fig. 9**, **Table S7**). The response of Pik-1 to AVR-Mgk1 was
345 previously overlooked; this illustrates the challenge of unravelling complex gene-for-gene interactions using
346 classical genetic approaches and highlights the dynamic nature of the co-evolution between an NLR
347 integrated domain and multiple families of effector proteins. As illustrated in Figure 9, our understanding of
348 the interactions between *M. oryzae AVR* effectors and rice disease resistance genes has transcended Flor's
349 single gene-for-gene model and involves network-type complexity at multiple levels [2–5].
350
351 **Why was the response of Pik-1 to AVR-Mgk1 previously overlooked?**
352
353 Despite its recognition by multiple Pik proteins, AVR-Mgk1 had not been discovered by previous studies.
354 This is mainly because *AVR-Mgk1* sequences are rare among the available *M. oryzae* genome sequences
355 (**Table S6**). In addition, the mini-chromosome encoding *AVR-Mgk1* appears to be absent from many isolates,
356 and thus has no homologous chromosome sequence to recombine with. Our TH3o x O23 cross resulted in
357 constantly similar significant *p*-values in the genetic association analysis (**Fig. 4C**). The mini-chromosome
358 is also affected by segregation distortion, resulting in a lower-than-expected frequency of *AVR-Mgk1*
359 inheritance in the F_1 progeny (**Fig. S4A**). Lastly, the mini-chromosome of the O23 isolate carries two distinct
360 *AVR* genes, *AVR-Mgk1* (two copies) and *AVR-PikD_O23*, which are both recognized by a single *Pik-1*
361 resistance gene (**Fig. 4C** and **S8**). *AVR-Mgk1* and *AVR-PikD_O23* mask each other's activities and are tightly
362 linked on the mini-chromosome, which is unfavourable for identification using classical genetic approaches.
363
364 Another challenge for identifying *AVR-Mgk1* was that the rice *Pish* locus, which confers resistance to O23
365 and TH3o, is also present in the rice cultivar Hitomebore (which contains *Piks*) (**Fig. 2B** and **2C**). Thus, this
366 network of gene-for-gene interactions was complicated by mutually masking *AVR* genes as well as by
367 stacked and paired rice resistance genes. Disentangling the overlapping contributions of these resistance loci
368 required rice RILs lacking the *Pish* locus (**Fig. 2**). Therefore, unravelling complex networks of gene-for-
369 gene interactions requires multiple-organism genetic approaches. This also demonstrates that to fully exploit
370 genetic resistance, we need to go beyond the 'blind' approach of breeding and deploying *R* genes in
371 agricultural crops without knowledge of the identity and population structure of the *AVR* genes encoding the
372 effectors they are potentially sensing.
373
374 **The *AVR-Mgk1* genes are flanked by retrotransposon sequences**
375
376 We observed deletion of *AVR-Mgk1* genes in one out of 144 sexual recombinants in just one generation.
377 This event was mediated by the tandemly duplicated *Inago2* retrotransposon sequences that flank the *AVR-*
378 *Mgk1* genes (**Fig. 5A**). We hypothesize that this type of repeat sequence-mediated deletion of *AVR* genes
379 might occur frequently in nature. The *M. oryzae* effector gene *AVR-Pita*, which occurs on the same mini-

380 chromosome as *AVR-Mgk1* and *AVR-PikD_O23*, is also flanked by the solo long terminal repeats (solo-
381 LTRs) of the retrotransposons *Inago1* and *Inago2* near the telomeric end of the chromosome [46] opposite
382 of *AVR-Mgk1* and *AVR-PikD_O23* (**Fig. 4C**). Chuma et al. proposed that the linkage of *AVR-Pita* to
383 retrotransposons is associated with translocation between different *M. oryzae* isolates, and therefore, may
384 facilitate horizontal gene transfer and recovery, particularly in asexual lineages [46]. This effector gene–
385 retrotransposon linkage could enable persistence of the effector gene in the fungal population despite
386 repeated deletions, and is a potential mechanism underpinning the two-speed genome concept [112–114]. In
387 the case of *AVR-Mgk1*, *Inago2* and dense solo-LTRs located between the two *AVR-Mgk1* copies (**Fig. 5A**)
388 appear to contribute to the effector gene's genetic instability and may explain its low frequency in *M. oryzae*
389 populations.
390
391 **AVR-Mgk1 is predicted to adopt a MAX fold structure**
392
393 Despite the primary sequence dissimilarity between AVR-Mgk1 and AVR-Pik, AlphaFold2 [103] predicted
394 that AVR-Mgk1 adopts a MAX fold structure (**Fig. 6C**) similar to AVR-Pik and several other *M. oryzae*
395 effectors [26–29,34]. However, the region that includes the highly polymorphic residues of AVR-Pik
396 effectors, which determine their binding to the HMA domain of Pik-1 and are modulated by arms race co-
397 evolution [69,70,92], differs structurally in AVR-Mgk1 (**Fig. 6C** and **6D**). This suggests that AVR-Mgk1
398 may bind the HMA domain through a different interface from AVR-Pik as demonstrated for other MAX
399 effectors [71,73,74,111]. This is supported by the observation that the Piks polymorphisms, which alter
400 binding to AVR-PikD, do not affect the interaction with AVR-Mgk1 (**Fig. 8**). It is remarkable that *M. oryzae*
401 effectors may have evolved to bind the HMA domain through multiple interfaces, which necessitates
402 additional structural studies of effector–HMA complexes.
403
404 **Identification of AVR-Mgk1 highlights flexible and complex host–pathogen recognition by an**
405 **integrated domain**
406
407 The identification of AVR-Mgk1 expands our understanding of the interaction between the integrated HMA
408 domains of rice NLR receptors and MAX effectors (**Fig. 9**). Pik proteins Pikm, Pik*, and Pikp detect and
409 bind AVR-Mgk1 and AVR-PikD via the Pik-1 integrated HMA domain (**Fig. S7** and **S11-15**). The
410 recognition of multiple MAX effectors by an NLR receptor was reported in the rice NLR pair Pia [68]. The
411 sensor NLR Pia-2 (RGA5) also contains the HMA domain, which binds the sequence-unrelated MAX
412 effectors AVR-Pia and AVR1-CO39 [68,73,74]. The presence of the HMA domain in Pik proteins also
413 enables Pikp to weakly respond to AVR-Pia, while this response is not observed with the combination of
414 Pikm and AVR-Pia [111]. These reports indicate that an integrated domain can flexibly recognize multiple
415 pathogen effectors. Our findings further extend the knowledge of HMA-mediated MAX effector recognition
416 in that the recognition specificity of AVR-Mgk1 is different from that of previously identified MAX effectors,
417 such as AVR-PikD, AVR-Pia, and AVR1-CO39 (**Fig. 9**). The AVR-Mgk1- and AVR-PikD-interacting
418 interfaces of the Pik HMA domain likely differ (**Fig. 6** and **8**). These different modes of interactions would

419 enable an HMA domain to target multiple effectors, and therefore contribute to a broad recognition spectrum
420 for pathogen effectors.
421
422 In the interactions between Pik proteins and AVR-Pik effectors, only a few polymorphisms dynamically
423 change the recognition spectrum and determine the recognition specificity [69–72,92]. Here, we
424 demonstrated that Piks binds and responds to AVR-Mgk1, but not to AVR-PikD (**Fig. 7**). This unique
425 recognition spectrum of Piks among other Pik family proteins (**Fig. 9**) is caused by two amino acid changes
426 (E229Q and A261V) relative to its quasi-identical protein Pikm (**Fig. 8**). We could not unambiguously
427 reconstruct the ancestral state and evolutionary trajectory of these two key polymorphisms because they are
428 recurrently polymorphic among Pik-1 proteins. However, considering that these polymorphisms between
429 Piks-1 and Pikm-1 have arisen among cultivated rice, Piks-1 may have lost the capacity to respond to AVR-
430 PikD as a trade-off between Pik immunity and rice yield, as reported for another rice resistance gene, *Pigm*
431 [115].
432
433 Collectively, our findings imply the potential of integrated HMA domains to flexibly recognize pathogen
434 effectors. In parallel, arms race co-evolution with *M. oryzae* and agricultural selection generate HMA domain
435 variants with different recognition specificities, which results in a network of tangled gene-for-gene
436 interactions between integrated HMA domains and MAX effectors (**Fig. 9**). HMA–effector interactions can
437 be a model to understand the flexible and complex mechanisms of host–pathogen recognition established
438 during their co-evolution.
439
440
441 ## Materials and Methods
442
443 ### *Magnaporthe oryzae* isolates O23 and TH3o and their genetic cross
444
445 The *Magnaporthe oryzae* isolates used in this study were imported to Japan with permission from the
446 Ministry of Agriculture, Forest and Fishery (MAFF), Japan and are maintained at Iwate Biotechnology
447 Research Center under the license numbers "TH3: MAFF directive 12 yokoshoku 1139" and "O23: MAFF
448 directive 51 yokoshoku 2502". Genetic crosses of the *M. oryzae* isolates TH3o (subculture of TH3) and O23
449 (O-23IN [PO12-7301-2]) [46] were performed as previously described [116]. Briefly, perithecia were
450 formed at the intersection of mycelial colonies of TH3o and O23 on oatmeal agar medium (20 g oatmeal, 10
451 g agar, and 2.5 g sucrose in 500 ml water) in a Petri dish during 3–4 weeks of incubation at 22°C under
452 continuous fluorescent illumination. Mature perithecia were crushed to release asci, which were transferred
453 to a water agar medium (10 g of agar in 500 ml of water) with a pipette. Each ascus was separated with a
454 fine sterilized glass needle under a micromanipulator. After 24 h incubation, germinated asci were
455 transferred to potato dextrose agar (PDA) slants. After two weeks incubation, the resulting mycelial colonies
456 were used for spore induction, and the spore solution was diluted and spread on PDA medium. After a 1-

457 week incubation, a mycelial colony derived from a single spore was transferred and used as an F_1 progeny
458 of TH3o and O23. For long-term storage, the F_1 progeny was grown on sterilized barley (*Hordeum vulgare*)
459 seeds in vials at 25°C for one month and kept in a case with silica gel at 10°C.
460
461 ***M. oryzae* infection assays**
462
463 For infection assay, rice plants one month after sowing were used. *M. oryzae* isolates TH3o, O23, and their
464 F_1 progeny were grown on oatmeal agar medium [40% oatmeal (w/v), 5% sucrose (w/v), and 20% agar
465 (w/v)] for two weeks at 25°C. Then aerial mycelia were washed off by rubbing mycelial surfaces with plastic
466 tube, and the colonies were incubated under black light (FL15BLB; Toshiba) for 3 to 5 days to induce
467 conidiation. Resulting conidia were suspended in distilled water, and adjusted to the concentration of $5 \times$
468 10^5 spores per ml. The conidial suspension was inoculated onto the press-injured sites on rice leaves. The
469 inoculated plants were incubated under dark at 28°C for 20 h, and then transferred to a growth chamber at
470 28°C with a 16-h light/8-h dark photoperiod. Disease lesions were photographed 10–12 days after
471 inoculation. The vertical lesion length was measured.
472
473 **Sequencing of rice cultivars Hitomebore and Moukoto and RILs derived from their cross**
474
475 We re-sequenced rice (*Oryza sativa*) lines Hitomebore and Moukoto and 249 RILs from their cross. First,
476 genomic DNA was extracted from fresh leaves using Agencourt Chloropure Kit (Beckman Coulter, Inc, CA,
477 USA). Then, DNA was quantified using Invitrogen Quant-iT PicoGreen dsDNA Assay Kits (Thermo Fisher
478 Scientific, MA, USA). For Hitomebore and Moukoto, library construction was performed using TruSeq
479 DNA PCR-Free Library Prep Kit (Illumina, CA, USA). These two libraries were sequenced using the
480 Illumina NextSeq, HiSeq, and MiSeq platforms (Illumina, CA, USA) for 75-bp, 150-bp, and 250/300-bp
481 paired-end reads, respectively (**Table S1**). For the 249 RILs, library construction was performed using
482 house-made sequencing adapters and indices. These libraries were sequenced using the Illumina NextSeq
483 platform for 75 bp paired-end reads (**Table S1**). First, we removed adapter sequences using FaQCs v2.08
484 [117]. Then, we used PRINSEQ lite v0.20.4 [118] to remove low-quality bases with the option "-trim_left 5
485 -trim_qual_right 20 -min_qual_mean 20 -min_len 50." In addition, 300-bp reads were trimmed to 200 bp by
486 adding an option "-trim_to_len 200."
487
488 **SNP calling for the rice RIL population**
489
490 The quality-trimmed short reads of the two parents and 249 RILs were aligned to the reference genome of
491 Os-Nipponbare-Reference-IRGSP-1.0 [119] using bwa mem command in BWA v0.7.17 [120] with default
492 parameters. Using SAMtools v1.10 [121], duplicated reads were marked, and the alignments were sorted in
493 positional order. These BAM files were subjected to variant calling. First, we performed valiant calling for
494 the parent cultivars Hitomebore and Moukoto according to the "GATK Best Practices for Germline short

495 variant discovery" [122] (https://gatk.broadinstitute.org/), which contains a BQSR step, two variant calling
496 steps with HaplotypeCaller in GVCF mode and GenotypeGVCFs commands, and a filter valiant step with
497 VariantFiltration command with the option "QD < 2.0 || FS > 60.0 || MQ < 40.0 || MQRankSum < -12.5 ||
498 ReadPosRankSum < -8.0 || SOR > 4.0." In the resulting VCF file, we only retained biallelic SNPs where: 1)
499 both parental cultivars had homozygous alleles, 2) the genotypes were different between Hitomebore and
500 Moukoto, and 3) both parental cultivars had a depth (DP) of eight or higher. As a result, 156,503 SNP
501 markers were extracted, and the position of these SNPs was converted to a bed file (position.bed) using the
502 BCFtools query command. For SNP genotyping of the 249 RILs, the VCF file was generated as follows: 1)
503 BCFtools v1.10.2 [123] mpileup command with the option "-t DP,AD,SP -A -B -Q 18 -C 50 -uv -l
504 position.bed"; 2) BCFtools call command with the option "-P 0 -A -c -f GQ"; 3) BCFtools filter command
505 with the option "-v snps -i 'INFO/MQ>=0 & INFO/MQ0F<=1 & AVG(GQ)>=0" ; 4) BCFtools norm
506 command with the option "-m+both. " Finally, we imputed the variants based on Hitomebore and Moukoto
507 genotypes using LB-impute [124].
508
509 ***De novo* assembly of the Hitomebore genome**
510
511 To reconstruct the *Pish* and *Pik* regions in Hitomebore, we performed a *de novo* assembly using Nanopore
512 long reads and Illumina short reads. To extract high-molecular-weight DNA from leaf tissue for nanopore
513 sequencing, we used the NucleoBond high-molecular-weight DNA kit (MACHEREY-NAGEL, Germany).
514 After DNA extraction, low-molecular-weight DNA was eliminated using the Short Read Eliminator Kit XL
515 (Circulomics, Inc, MD, USA). Then, following the manufacturer's instructions, sequencing was performed
516 using Nanopore PromethION (Oxford Nanopore Technologies [ONT], UK). First, base-calling of the
517 Nanopore long reads was performed for FAST5 files using Guppy 3.4.5 (ONT, UK), converted to FASTQ
518 format (**Table S1**). The lambda phage genome was removed from the generated raw reads with NanoLyse
519 v1.1.0 [125]. We then trimmed the first 50 bp of each read and filtered out reads with an average read quality
520 score of less than seven and reads shorter than 3,000 bases with NanoFilt v2.7.1 [125]. Next, the Nanopore
521 long reads were assembled using NECAT v0.0.1 [126] setting the genome size to 380 Mbp. To further
522 improve the accuracy of assembly, Racon v1.4.20 [127] was used twice for error correction, and Medaka
523 v1.4.1 (https://github.com/nanoporetech/medaka) was subsequently used to correct mis-assembly.
524 Following this, two rounds of consensus correction were performed using bwa-mem v0.7.17 [120] and HyPo
525 v1.0.3 [128] with Illumina short reads. We subsequently removed haplotigs using purge-haplotigs v1.1.1
526 [129], resulting in a 374.8 Mbp *de novo* assembly comprising 77 contigs. This assembly was further
527 scaffolded with RagTag v1.1.0 [130], with some manual corrections, using the Os-Nipponbare-Reference-
528 IRGSP-1.0 as a reference genome. The resulting Hitomebore genome sequence was deposited on Zenodo
529 (https://doi.org/10.5281/zenodo.6839127).
530
531 **RNAi-mediated knockdown of *Piks-1* and *Piks-2* in rice**
532

533 To prepare *Piks-1* and *Piks-2* knockdown vectors, the cDNA fragments Piks-1A (nt 618–1011) and Piks-1B
534 (nt 1132–1651) for *Piks-1*, and Piks-2A (nt 121–524) and Piks-2B (nt 2317–2726) for *Piks-2* were amplified
535 using primer sets (KF852f/KF853r, KF854f/KF855r, KF848f/KF849r, and KF801f/KF802r, respectively,
536 **Table S8**). The resulting PCR products were cloned into the Gateway vector pENTR-D-TOPO (Invitrogen,
537 Carlsbad, CA, USA), and transferred into the pANDA vector [131] using LR clonase (Invitrogen), resulting
538 in pANDA-Piks-1A, pANDA-Piks-1B, pANDA-Piks-2A, and pANDA-Piks-2B. Plasmids were
539 transformed into *Agrobacterium tumefaciens* (EHA105) and used for stable transformation of rice RIL #58
540 (*Piks* +) by *Agrobacterium*-mediated transformation. Transformation and regeneration of rice plants were
541 performed according to Hiei et al. [132].
542
543 To determine *Piks-1* and *Piks-2* expression in the transgenic lines, reverse transcription quantitative PCR
544 (RT-qPCR) was performed. Total RNA was isolated from transformant leaves using the Qiagen RNeasy
545 plant mini kit (Qiagen, Venlo, the Netherlands). cDNA was synthesized with the ReverTra Ace kit
546 (TOYOBO, http://www.toyobo.co.jp) and used as a template for quantitative PCR (qPCR) using primer sets
547 (YS29f/YS30r for *Piks-1*, YS35f/YS36r for *Piks-2*, Actin-RTf/Actin-RTr for rice *Actin*, **Table S8**). qPCR
548 was performed using the Luna Universal qPCR Master Mix (New England Biolabs Japan, Tokyo, Japan) on
549 a QuantStudio 3 Real-Time PCR System (Thermo Fisher Scientific, MA, USA). The relative expression
550 levels of *Piks*-1 and *Piks*-2 were calculated via normalization with rice *Actin*.
551
552 **Phylogenetic analysis of Pik alleles**
553
554 The sequences of *Pik-1* (*Pikh-1* [AET36549.1], *Pikp-1* [ADV58352.1], *Pik*-1* [ADZ48537.1], *Pikm-1*
555 [AB462324.1], and *Piks-1* [AET36547.1]) and *Pik-2* (*Pikh-2* [AET36550.1], *Pikp-2* [ADV58351.1], *Pik*-2*
556 [ADZ48538.1], *Pikm-2* [AB462325.1], and *Piks-2* [AET36548.1]) were aligned using MAFFT v7.490 [133]
557 with the option "--globalpair --maxiterate 1000". The phylogenetic trees of *Piks-1* and *Piks-2* were separately
558 drawn based on nucleotide sequences with IQ-TREE v2.0.3 [134] using 1,000 ultrafast bootstrap replicates
559 [135]. The models for reconstructing trees were automatically selected by ModelFinder [136] in IQ-TREE.
560 ModelFinder selected "HKY+F" for *Pik-1* and "F81+F" for *Pik-2* as the best-fit models according to the
561 Bayesian information criterion (BIC). Finally, the midpoint rooted trees were drawn with FigTree v1.4.4
562 (http://tree.bio.ed.ac.uk/software/figtree/).
563
564 **Sequencing of *M. oryzae* isolates O23 and TH3o and their F_1 progeny**
565
566 For long-read sequencing, O23 and d44a genomic DNA was extracted from liquid-cultured aerial hyphae
567 using the NucleoBond high-molecular-weight DNA kit (MACHEREY-NAGEL, Germany). The genomic
568 DNA was processed through the short-read eliminator kit XL (Circulomics). The filtered genomic DNA (2
569 μg) was used to construct a library for Nanopore sequencing using the ligation sequencing kit SQK-LSK109

570 (ONT, UK). Sequencing was performed using the MinION system with a FLO-MIN106D (R9.4) flow cell
571 (ONT, UK).
572
573 TH3o genomic DNA was extracted using the cetyl trimethyl ammonium bromide (CTAB) method. The
574 extracted DNA was purified using Genomic-tip (Qiagen, Germany) according to the manufacturer's protocol.
575 Sequencing was performed by Macrogen, Inc., Seoul, Korea, using the PacBio RS II sequencer (Pacific
576 Biosciences of California, Inc., Menlo Park, CA, USA).
577
578 For short-read sequencing of O23, TH3o, and their F_1 progeny, genomic DNA was extracted from aerial
579 hyphae using the NucleoSpin Plant II Kit (Macherey Nagel). Libraries for paired-end short reads were
580 constructed using an Illumina TruSeq DNA LT Sample Prep Kit (Illumina, CA, USA). The paired-end
581 library was sequenced by the Illumina NextSeq platform (Illumina, CA, USA). We also sequenced O23
582 genomic DNA using the MiSeq platform to polish the *de novo* O23 assembly.
583
584 The adapters of short-reads were trimmed by FaQCs v2.08 [117]. In this step, we also filtered the reads and
585 discarded reads shorter than 50 bases and those with an average read quality below 20.
586
587 ***De novo* assembly of O23, TH3o, and d44a genomes**
588
589 First, base-calling of the Nanopore long reads was performed for FAST5 files of O23 and d44a with Guppy
590 3.4.4 (ONT, UK). The lambda phage genome was removed from the generated raw reads with NanoLyse
591 v1.1.0 [125]. We then trimmed the first 50 bp of each read and filtered out reads with an average read quality
592 score of less than 7 and reads shorter than 3,000 bases with NanoFilt v2.7.1 [125]. The quality-trimmed
593 Nanopore long reads of O23 and d44a were assembled with NECAT v0.0.1 [126] setting the genome size to
594 42 Mbp. The assembled contigs were then polished with medaka v0.12.1
595 (https://github.com/nanoporetech/medaka) and with Hypo v1.0.3 [128]. In Hypo, we used MiSeq and
596 NextSeq short-reads for O23 and d44a, respectively, in addition to quality-trimmed Nanopore long reads.
597
598 For the *de novo* assembly of TH3o, we trimmed the first 50 bp of each read and filtered out reads with an
599 average read quality score of less than 7 and reads shorter than 2,000 bases with NanoFilt v2.7.1 [125]. The
600 quality-trimmed PacBio long reads of TH3o were assembled with MECAT v2 [137] setting the genome size
601 to 42 Mbp. The assembled contigs were polished with Hypo v1.0.3 [128] using NextSeq short-reads and
602 PacBio long reads of TH3o.
603
604 To evaluate the completeness of the gene set in the assembled contigs, we applied BUSCO analysis v3.1.0
605 [95]. For BUSCO analysis, we set "genome" as the assessment mode, and *Magnaporthe grisea* was used as
606 the species in AUGUSTUS [138]. *Sordariomyceta* odb9 was used as the dataset.
607

608 The genome sequences of the *M. oryzae* isolates 70-15 (MG8 genome assembly in
609 https://fungi.ensembl.org/Magnaporthe_oryzae/Info/Index) [96], O23, TH3o, and d44a were compared by
610 dot plot analysis of D-GENIES [139]. The chromosome sequences of O23 and d44a were numbered and
611 ordered based on those of 70-15.
612
613 **Variant calling for the *M. oryzae* F_1 progeny derived from a cross between O23 and TH3o**
614
615 Quality-trimmed short-reads were aligned to the O23 reference genome using the bwa mem command in
616 BWA v0.7.17 with default parameters [120]. Using SAMtools v1.10 [121], duplicated reads were marked
617 and the alignments were sorted to positional order. Only properly paired and uniquely mapped reads were
618 retained using SAMtools [121]. For SNP markers on core chromosomes (chromosomes 1–7), the VCF file
619 was generated as follows: 1) BCFtools v1.10.2 [123] mpileup command with the option "-a AD,ADF,ADR
620 -B -q 40 -Q 18 -C 50"; 2) BCFtools call command with the option "-vm -f GQ,GP --ploidy 1"; 3) BCFtools
621 filter command with the option "-i "INFO/MQ>=40". In the VCF file, biallelic SNPs were retained only
622 where: 1) O23 had the same genotype as the O23 reference genome, 2) both parental isolates, O23 and TH3o,
623 had a depth (DP) of four or higher, 3) the average genotype quality (GQ) across all the samples was 100 or
624 higher, 4) the number of missing genotypes among the 144 F_1 progeny was less than 15, and 5) the allele
625 frequency was between 0.05 and 0.95. As a result, 7,867 SNP markers were extracted from the core
626 chromosomes. For presence/absence markers on the remaining contigs, we selected candidate
627 presence/absence regions on the parental genomes, O23 and TH3o. First, the BCFtools mpileup command
628 was used only for the BAM files of O23 and TH3o with the option "-a DP -B -q 40 -Q 18 -C 50". Second,
629 BCFtools view command was used with the option "-g miss -V indels" to extract the positions where either
630 O23 or TH3o was missing. Third, only the positions where O23 had a depth of eight or higher and TH3o
631 had a depth of zero were retained. These positions were concatenated using the bedtools v2.29.2 [140] merge
632 command with the option "-d 10". Only candidate regions larger than or equal to 50 bp were retained. Using
633 the SAMtools bedcov command with the option "-Q 0", the number of alignments of each F_1 progeny on
634 these candidate regions was counted. If an F_1 progeny had at least one alignment on a candidate region, the
635 F_1 progeny was considered to have a presence-type marker for that region. On the other hand, if an F_1
636 progeny had no alignment on a candidate region, the F_1 progeny was considered to have an absence-type
637 maker for that region. Finally, only the presence/absence markers that 1) had an average depth of four or
638 higher for O23 regions, and one or less for TH3o regions, and 2) had an allele frequency between 0.05 and
639 0.95 were retained. As a result, 265 presence/absence markers were extracted for the remaining contigs.
640
641 **Annotation of the O23 reference genome**
642
643 The segregation distortion of each marker was tested by a two-sided binomial test (p = 0.5). O23-specific
644 regions were annotated by aligning TH3o contigs to the O23 reference genome with Minimap2 [141] using
645 the option "-x asm5". The recombination frequency of core chromosomes in F_1 progeny was calculated by

646 MSTmap [142] with the parameter set described in [143] except for "missing_threshold 1". The calculated
647 recombination frequency was smoothed by the 1-D smoothing spline "UnivariateSpline" function in the
648 "SciPy" python library, and absolute Δ centiMorgans were sampled at every 30 kbp. Transposable elements
649 were annotated by EDTA v1.9.0 [144] with the option "--anno 1 --species others --step all". Coding
650 sequences of the genome assembly version MG8 of the *M. oryzae* isolate 70-15 [96] and the library of
651 transposable elements curated in Chuma et al. [46] were also provided as input to EDTA. We only retained
652 the annotations from the provided transposable elements. LTRs of retrotransposons were also annotated by
653 EDTA, independently. The genes on the O23 reference genome were annotated by aligning the coding
654 sequences of the genome assembly version MG8 of 70-15 using Spaln2 v2.3.3 [145]. The sequence similarity
655 of the mini-chromosome sequence O23_contig_1 was analysed against the O23 core chromosomes using
656 Minimap2 [141] with the option "-x asm5". We filtered out the alignments shorter than 1 kbp or with a
657 mapping quality less than 40. Finally, these sequence similarities were plotted by Circos (http://circos.ca/)
658 including other genomic features. For gene density, the overlapped gene annotations were regarded as a
659 single gene annotation.
660
661 **Association analysis between genetic markers and phenotype**
662
663 The association between the genetic markers and the phenotype was evaluated using the R package rrBLUP
664 [146]. To correct the threshold of *p*-values for multiple testing, false discovery rate was used for the rice
665 RILs and *M. oryzae* F_1 progeny. For false discovery rate, the "multipletests" function in the "statsmodels"
666 python library was used with the option "method: fdr_bh, alpha: 0.01".
667
668 **RNA-seq to identify *AVR-Mgk1***
669
670 Total RNA of TH3o and O23 was extracted at different stages (24 and 48 h) of barley infection using the
671 SV Total RNA Isolation System (Promega, WI, USA). One microgram of total RNA was used to prepare
672 each sequencing library with the NEBNext Ultra II Directional RNA library prep kit (New England Biolabs
673 Japan, Tokyo, Japan) following the manufacturer's protocol. The library was sequenced by paired-end mode
674 using the Illumina Hiseq X platform (Illumina, CA, USA).
675
676 For quality control, the reads were filtered and reads shorter than 50 bases and those with an average read
677 quality below 20 and trimmed poly(A) sequences were discarded with FaQCs v2.08 [117]. The quality-
678 trimmed reads were aligned to the O23 reference genome with HISAT2 v2.1 [147] with the options "--no-
679 mixed --no-discordant --dta". BAM files were sorted and indexed with SAMtools v1.10 [121], and transcript
680 alignments were assembled with StringTie v2.0 [148] separately for each BAM file.
681
682 **Transformation of *M. oryzae* isolate Sasa2 with *AVR-Mgk1* and *AVR-PikD_O23***
683

684 To construct the *pCB1531-pex22p-AVR-Mgk1* expression vector, *AVR-Mgk1* was amplified by PCR using
685 primer sets XbaI_O23_48h.1149.1-F and BamHI_O23_48h.1149.1-R (**Table S8**) from cDNA of *M. oryzae*
686 O23-infected barley leaf material. The PCR product was digested with *Xba*I and *Bam*HI and ligated into the
687 *pCB1531-pex22p-EGFP* vector [17] using the *Xba*I and *Bam*HI sites to be exchanged with EGFP tag. To
688 construct the *pCB1531-pex22p-AVR-PikD'*(*AVR-Pik-D_O23*) expression vector, a 0.3-kb fragment
689 containing *AVR-PikD'* (*AVR-Pik-D_O23*) was amplified by PCR using the primers Xba1_kozak_pex31_U1
690 [17] and KF792r (**Table S8**) from *M. oryzae* O23 genomic DNA. The PCR product and *pCB1531-pex22p-*
691 *EGFP* expression vector were digested with *Xba*I and *Eco*RI to ligate *AVR-PikD_O23* into the position of
692 the EGFP tag, generating *pCB1531-pex22p-AVR-PikD'*(*AVR-Pik-D_O23*). The resulting vectors were used
693 to transform *M. oryzae* Sasa2 following a previously described method [149].
694
695 To confirm *AVR-Mgk1* expression in infected rice leaves, Sasa2 transformants were punch inoculated on
696 rice cultivar Moukoto. We reverse transcribed cDNA from RNA extracted from the infected rice leaves and
697 amplified *AVR-Mgk1* via PCR using primer sets listed in **Table S8**. Rice and *M. oryzae Actin* were used as
698 controls.
699
700 **Protein sequence alignment between AVR-Mgk1 and AVR-PikD**
701
702 NCBI BLAST (https://blast.ncbi.nlm.nih.gov/Blast.cgi) was used to align the AVR-Mgk1 and AVR-PikD
703 protein sequences using the Needleman-Wunsch algorithm [150] for pairwise global alignment using default
704 parameters.
705
706 **Clustering of putative *M. oryzae* AVR protein sequences using TRIBE-MCL**
707
708 A dataset of the putative *M. oryzae* effector proteins [31] amended with AVR-Mgk1 was clustered by
709 TRIBE-MCL [102] using "1e-10" for an E-value cut-off of BLASTP [151] and "1.4" for the inflation
710 parameter "-I" in mcl. The other parameters were default. The sequence set used in this analysis was
711 deposited in Zenodo (https://doi.org/10.5281/zenodo.6839127).
712
713 **AVR-Mgk1 structure prediction**
714
715 The AVR-Mgk1 structure was predicted using AlphaFold2 [103]. The signal peptide sequence in AVR-
716 Mgk1 was predicted by SignalP v6.0 (https://services.healthtech.dtu.dk/service.php?SignalP) [152]. The
717 amino acid sequence without the signal peptide (Arg25-Trp85) was used as an input for AlphaFold2 [103],
718 available on the Colab notebook. The best model generated by AlphaFold2 was visualised by ChimeraX
719 v1.2.5 [153] together with the protein structures of AVR-PikD (PDB ID: 6FU9 chain B) [70], AVR-Pia
720 (PDB ID: 6Q76 chain B) [111], and AVR1-CO39 (PDB ID: 5ZNG chain C) [74]. The protein structures of
721 AVR-Mgk1 and AVR-PikD were aligned by structure-based alignment using TM-align

722 (https://zhanggroup.org/TM-align) [104]. The AVR-Mgk1 structure predicted by AlphaFold2 is deposited
723 on Zenodo (https://doi.org/10.5281/zenodo.6839127).
724
725 **BLAST search of AVR-Mgk1 to the NCBI database**
726
727 To find sequences related to AVR-Mgk1, BLASTN and BLASTP searches were run against the non-
728 redundant NCBI database. A BLASTN search was also run against the whole-genome shotgun contigs of
729 *Magnaporthe* (taxid: 148303). For all analyses, default parameters were used.
730
731 **Assays for protein-protein interactions**
732
733 For the yeast two-hybrid assay, In-Fusion HD Cloning Kit (Takara Bio USA) was used to insert the *AVR-*
734 *Mgk1* fragment (Arg25-Trp85) into pGADT7 (prey) and pGBKT7 (bait). DNA sequences of the fragments
735 of AVR-PikD (Lys30-Phe113) and the Pik HMA domains (Piks-HMA [Gly186-Asp264], Pikp-HMA
736 [Gly186-Asp263], Pik*-HMA [Gly186-Asp264], and Pikm-HMA [Gly186-Asp264], defined in De la
737 Concepcion et al. [70]) were ligated into pGADT7 and pGBKT7 as described previously [69]. The primer
738 sets used for PCR amplification of the fragments are listed in **Table S8**. Yeast two-hybrid assays were
739 performed as described previously [69], except for the use of basal medium lacking leucine (L), tryptophan
740 (W), adenine (A), and histidine (H), but containing 5-Bromo-4-Chloro-3-Indolyl α-D-galactopyranoside (X-
741 α-gal) (Clontech) and 10 mM 3-amino-1,2,4-triazole (3AT) (Sigma) to detect interactions.
742
743 Co-IP experiments of transiently expressed proteins in *Nicotiana benthamiana* were performed as described
744 previously [69]. The protein regions used in the co-IP experiment were the same as those used in the yeast
745 two-hybrid assay. We used N-terminally tagged FLAG:AVR and HA:HMA. The lysates of AVRs and HMA
746 domains were diluted to compare the results at the same concentration and mixed (1:4, 1:2, or 1:1 ratio) *in*
747 *vitro* to assemble the protein complex. For co-IP of HA-tagged proteins, Anti-HA affinity gel (Sigma) was
748 used, and proteins were eluted by using 0.25 mg/ml HA peptide (Roche). HA- and FLAG-tagged proteins
749 were immunologically detected using HRP-conjugated anti-HA 3F10 (Roche) and anti-FLAG M2 (Sigma),
750 respectively. The primer sets used in this experiment are listed in **Table S8**.
751
752 **Hypersensitive response cell death assay in *N. benthamiana***
753
754 Transient gene expression in *N. benthamiana* was performed by agroinfiltration according to methods
755 described by van der Hoorn et al. [154]. Briefly, *A. tumefaciens* strain GV3101 pMP90 carrying binary
756 vectors was inoculated from glycerol stock in liquid LB supplemented with 30 µg/ml rifampicin, 20 µg/ml
757 gentamycin, and 50 µg/ml kanamycin and grown overnight at 28°C with shaking until saturation. Cells were
758 harvested by centrifugation at 2000 × g at room temperature for 5 min. Cells were resuspended in infiltration
759 buffer (10 mM $MgCl_2$, 10 mM MES-KOH pH 5.6, 200 µM acetosyringone) and diluted to the appropriate

760 OD_{600} (**Table S9** and also see [81,155]) in the stated combinations and left to incubate in the dark for 2 hours
761 at room temperature prior to infiltration into 5-week-old *N. benthamiana* leaves. Hypersensitive cell death
762 phenotypes were scored from 0 to 6 according to the scale in Maqbool et al. [28].
763
764
765 **Data Availability**
766
767 All the sequence data used in this study was deposited at European Nucleotide Archive (ENA,
768 https://www.ebi.ac.uk/ena/browser/home) and the DNA Data Bank of Japan (DDBJ,
769 https://www.ddbj.nig.ac.jp/index-e.html) with the study accessions PRJEB53625 and PRJDB13864,
770 respectively. The datasets used in this study are available at Github repository
771 (https://github.com/YuSugihara/Sugihara_et_al_2022) archived in Zenodo
772 (https://doi.org/10.5281/zenodo.6839127).
773
774
775 **Funding**
776
777 This study was supported by JSPS KAKENHI 15H05779, 20H05681 to RT, the Royal Society UK-Japan
778 International exchange grants JPJSBP120215702 and IEC\R3\203081 to RT, SK and MB, the Gatsby
779 Charitable Foundation (https://www.gatsby.org.uk/), the UK Research and Innovation Biotechnology and
780 Biological Sciences Research Council (UKRI-BBSRC) grants BB/P012574, BBS/E/J/000PR9797,
781 BBS/E/J/000PR9798 BB/R01356X/1, and the European Research Council (ERC) BLASTOFF grant 743165.
782
783
784 **Acknowledgements**
785
786 We thank Mauricio P. Contreras for valuable comments on the figures. We also thank Hiroe Utsushi, Akiko
787 Hirabuchi, Yukie Hiraka, and Mari Iwai at Iwate Biotechnology Research Center, Japan, for technical
788 support, and Phil Robinson at The Sainsbury Laboratory, UK for photography.
789
790
791
792
793
794
795
796
797

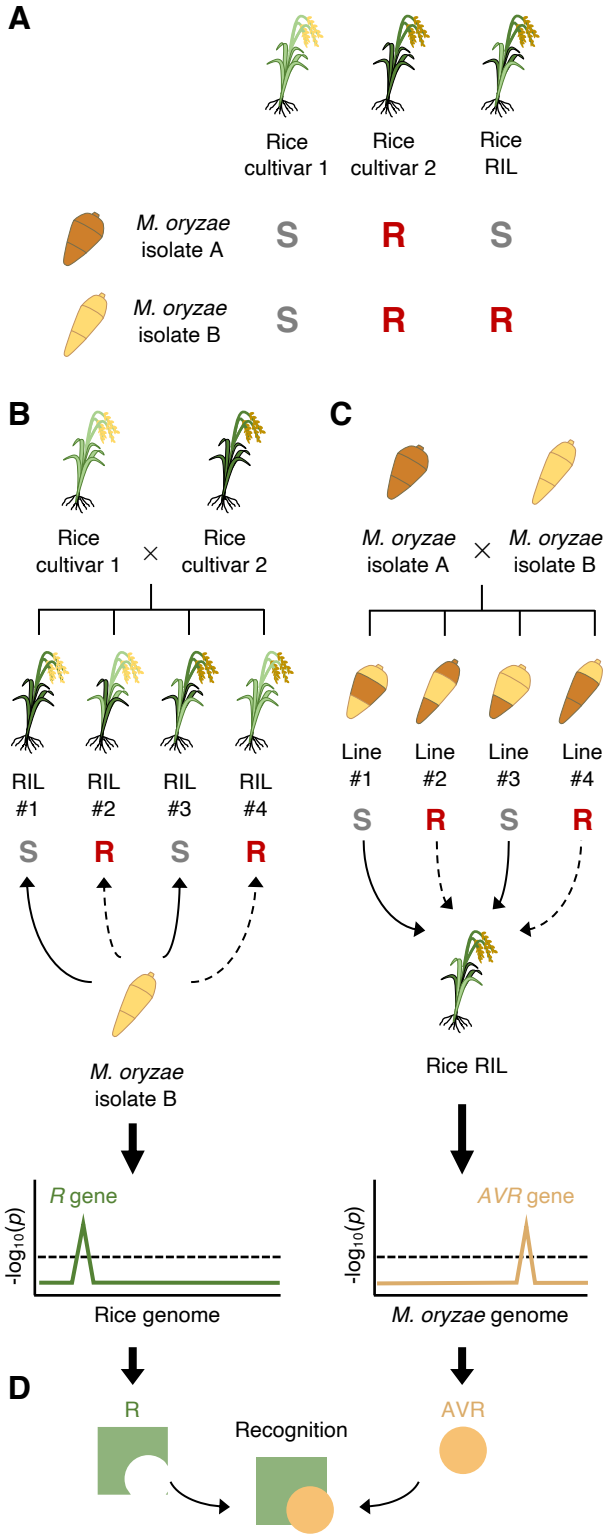

Fig. 1. Integrated host and pathogen genetic analyses reveal a previously overlooked gene-for-gene interaction. (A) Rice recombinant inbred lines (RILs) generated to genetically dissect rice resistance to different *M. oryzae* isolates. We generated RILs through self-pollination after the F_1 generation to reduce heterozygosity. (B) Rice genetics identifies a locus contributing to a rice resistance (*R*) to a *M. oryzae* isolate. (C) *Magnaporthe* genetics identifies a locus contributing to an avirulence (*AVR*) of a *M. oryzae* isolate to a rice cultivar. (D) Mechanistic studies confirm the gene-for-gene interaction between the identified *R* and *AVR* genes.

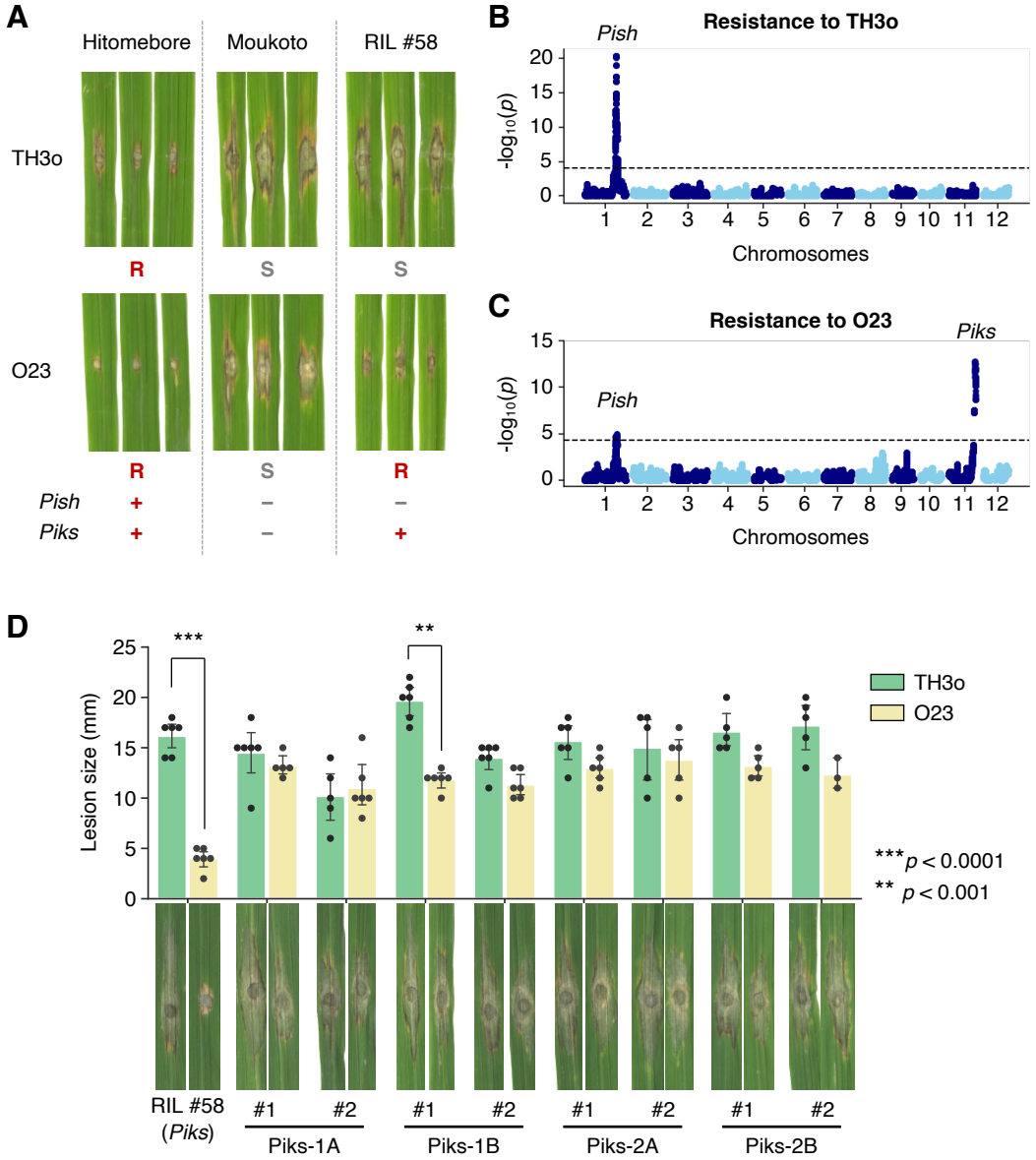

Fig. 2. Rice recombinant inbred lines (RILs) untangle the genetics of rice cultivar Hitomebore resistance to *M. oryzae* isolates TH3o and O23. (A) Punch inoculation assays using *M. oryzae* isolates TH3o and O23 on rice cultivars Hitomebore and Moukoto. Hitomebore is resistant (*R*) to TH3o and O23, while Moukoto is susceptible (*S*) to these isolates. RIL #58, one of the RILs produced from the cross between Hitomebore and Moukoto, is susceptible to TH3o but resistant to O23. (B) Genetic association analysis of rice RIL susceptibility to TH3o identified a locus containing the rice NLR resistance gene *Pish*. (C) Genetic association analysis of rice RIL susceptibility to O23 identified loci containing the rice NLR resistance genes *Pish* and *Piks*. We used 156,503 single nucleotide polymorphism (SNP) markers, designed from the parental genomes, for genetic association analysis on 226 RILs. The vertical axis indicates $-\log_{10}(p)$, where the *p*-value is how likely the marker shows association with a trait due to random chance. The dashed line shows the *p*-value corresponding to a false discovery rate of 0.01. (D) Punch inoculation assays of RNAi-mediated knockdown lines of *Piks-1* and *Piks-2* with the isolates TH3o and O23. We used RIL #58 (*Pish* -, *Piks* +) as the genetic background for the RNAi lines. For each *Pik* gene, we prepared two independent RNAi constructs targeting different regions on the gene (Piks-1A and Piks-1B for *Piks-1*, and Piks-2A and Piks-2B for *Piks-2*, **Fig. S1**). We performed punch inoculation assays using isolates TH3o and O23 with two RNAi lines per construct, along with RIL #58 as a control. The lesion size was quantified. Asterisks indicate statistically significant differences between TH3o and O23 (two-sided Welch's t-test).

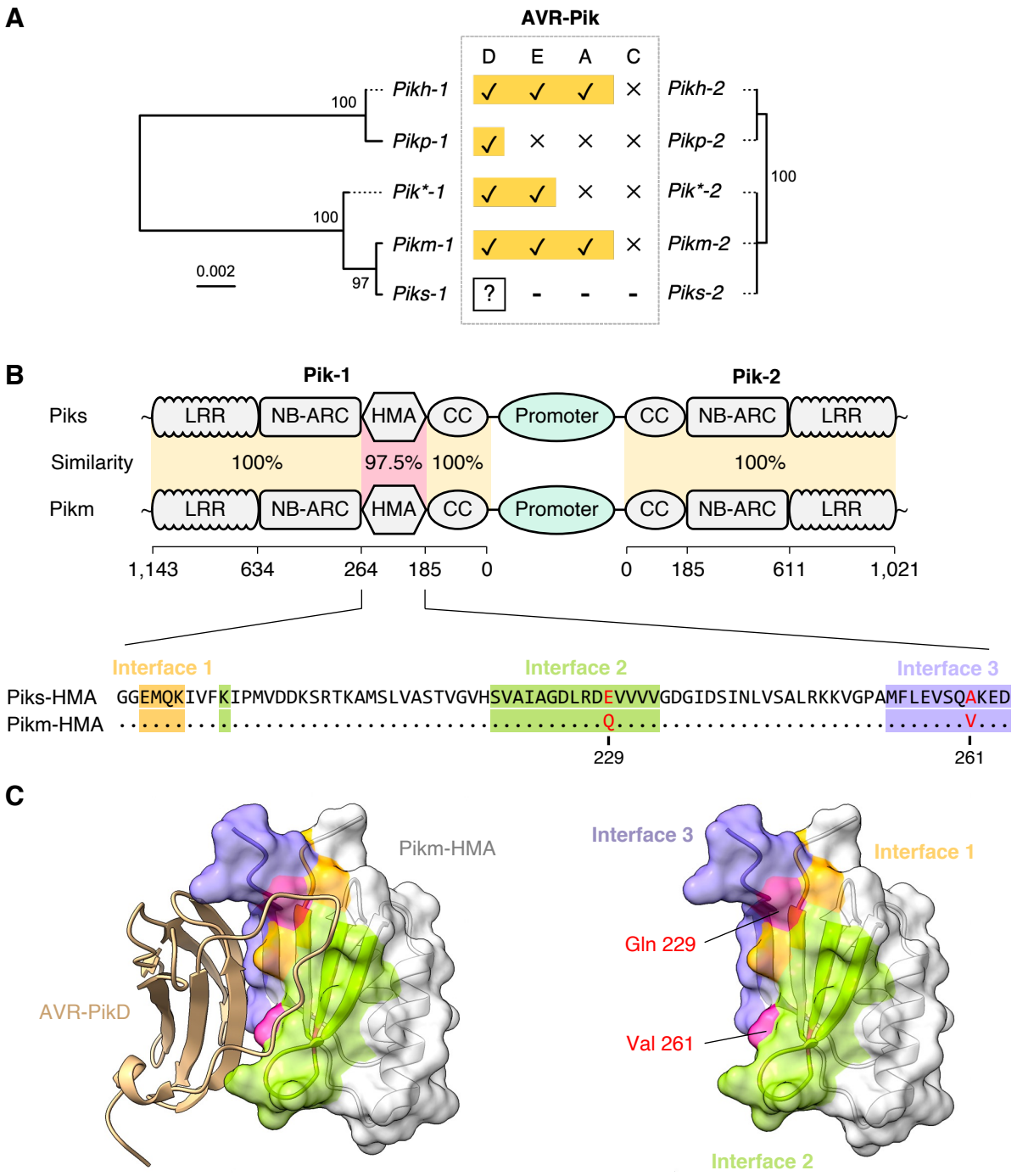

Fig. 3. Two amino acid replacements differentiate Piks-1 from Pikm-1. (A) Phylogenetic trees of *Pik* resistance gene alleles are shown together with the experimentally validated protein interactions between Pik and AVR-Pik allelic products. The phylogenetic trees of *Pik-1* and *Pik-2* were drawn based on nucleotide sequences, and show the closest genetic relationship between *Piks* and *Pikm*. (B) Schematic representations of the gene locations and domain architectures of the NLR pair genes *Pik-1* and *Pik-2*. The genetically linked Pik-1 and Pik-2 share a common promoter region. Pik-1 has a non-canonical integrated HMA domain that binds *M. oryzae* AVR-Pik allelic products. Piks and Pikm differ by two amino acid replacements located at the integrated HMA domain of Pik-1. These polymorphisms, E229Q and A261V, are located at the binding interface 2 and 3 for AVR-PikD, respectively [70]. We calculated the sequence identities between Piks and Pikm based on amino acid sequences. (C) Structure of Pikm-HMA (PDB ID: 6FU9 chain A) in complex with AVR-PikD (PDB ID: 6FU9 chain B) [70]. The two amino acids differing between Piks-HMA and Pikm-HMA are exposed to the AVR-PikD-interaction site. The colors correspond to the colors of the alignment in (B).

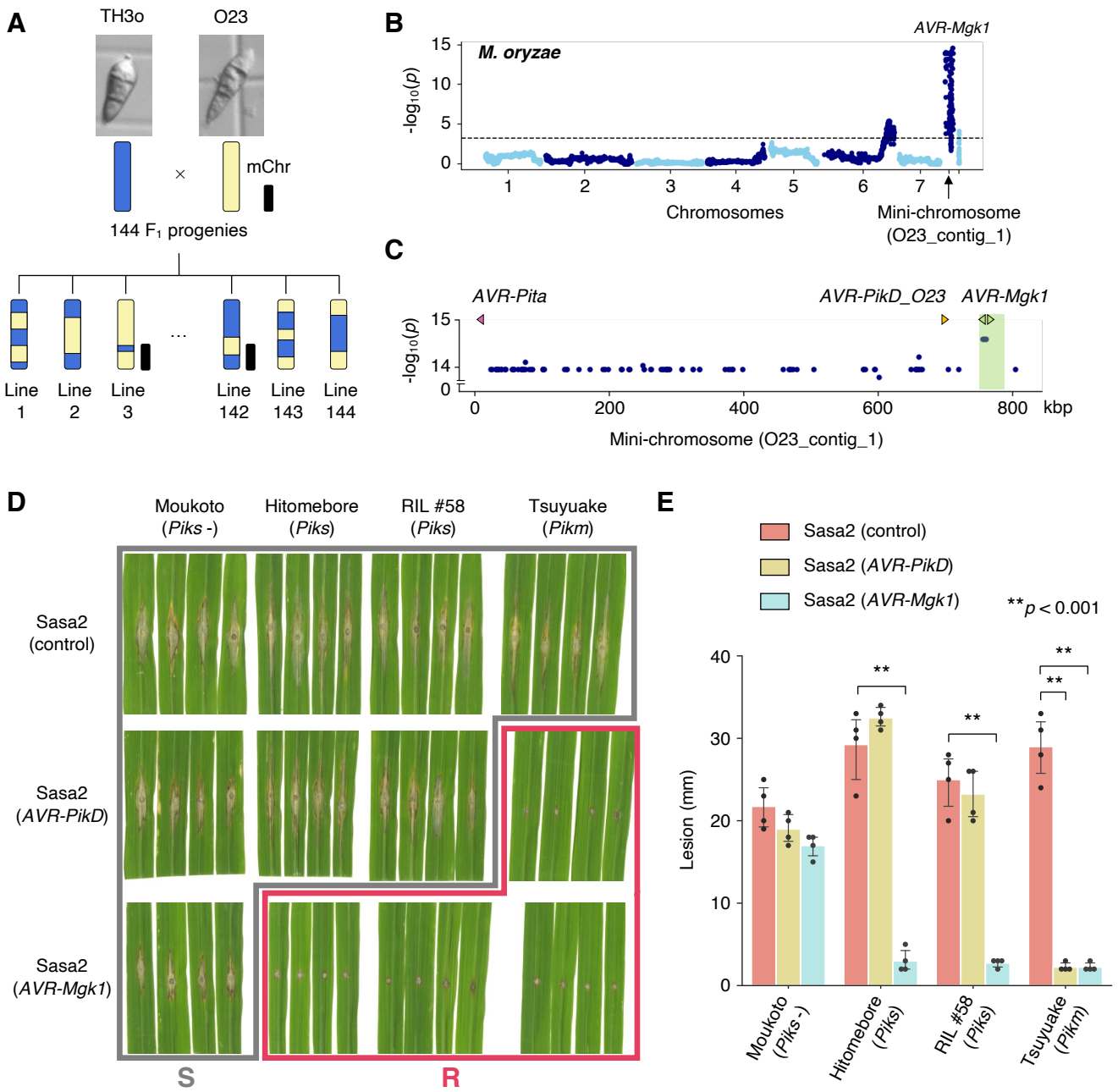

Fig. 4. *M. oryzae* genetic analysis identifies an *AVR* gene, *AVR-Mgk1*, encoded on a mini-chromosome. (A) Schematic representations of the F_1 progeny generated after a cross between *M. oryzae* isolates TH3o and O23. We subjected all F_1 progeny to whole-genome sequencing. O23 possesses a mini-chromosome [46]. (B) Genetic association of the TH3o x O23 F_1 progeny using infection lesion size on RIL #58 (*Pish* -, *Piks* +) rice plants as a trait. The vertical axis indicates $-\log_{10}(p)$, where the *p*-value is how likely the marker shows association with a trait due to random chance. The dashed line shows the *p*-value corresponding to a false discovery rate of 0.01. The association analysis based on the O23 reference genome identified *AVR-Mgk1*, encoded on the mini-chromosome sequence O23_contig_1, as an *AVR* gene. O23_contig_1 was not present in the TH3o genome and was unique to the O23 genome. We used 7,867 SNP markers for chromosomes 1–7 and 265 presence/absence markers for the other contigs. (C) *p*-values for O23_contig_1 with annotated *AVR*s. We also detected *AVR-Pita* and *AVR-PikD* in O23_contig_1. *AVR-PikD* in O23_contig_1 contains a frameshift mutation, so we named this variant *AVR-PikD_O23*. The region encoding two *AVR-Mgk1* genes and showing lower *p*-values is highlighted in green. Nucleotide sequences of the two *AVR-Mgk1* genes, arranged in a head-to-head orientation, are identical. (D) Results of punch inoculation assays using *M. oryzae* isolate Sasa2 transformed with *AVR-PikD* or *AVR-Mgk1*. Wild-type Sasa2 infected all the cultivars tested in this study. The Sasa2 transformant expressing *AVR-PikD* infected RIL #58 (*Piks*), but that expressing *AVR-Mgk1* did not infect RIL #58 (*Piks*) or Tsuyuake (*Pikm*) rice plants. (E) Quantification of the lesion size in (D). Asterisks indicate statistically significant differences ($p < 0.001$, two-sided Welch's t-test).

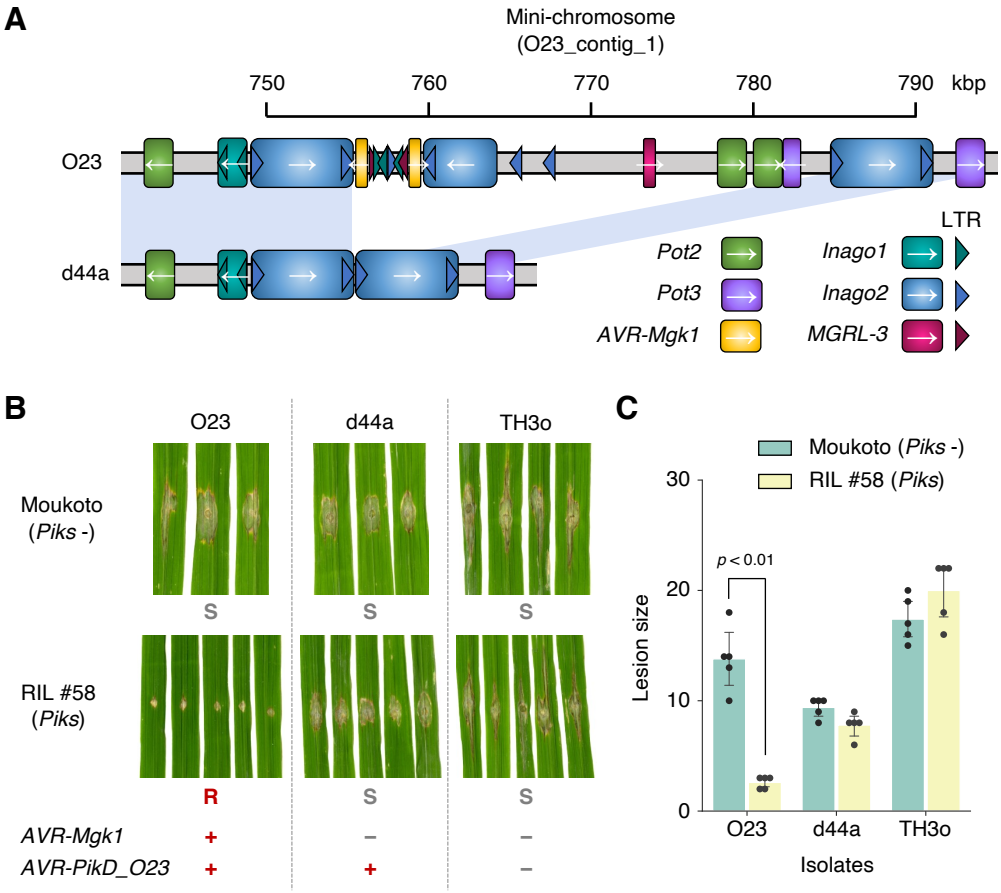

Fig. 5. *Inago2* retrotransposon repeat sequence-mediated deletion of *AVR-Mgk1* re-establishes virulence. (A) Comparison of the genomic structures around the *AVR-Mgk1* genes between *M. oryzae* isolates O23 and d44a; d44a is an F_1 progeny of TH3o x O23. d44a lost the two *AVR-Mgk1* genes. Sequences of transposable elements around *AVR-Mgk1* genes (*Pot2*, *Pot3*, *Inago1*, *Inago2*, and *MGRL-3*) are indicated by color-coded rectangles. Long terminal repeats (LTRs) of retrotransposons are shown in triangles. (B) d44a is virulent against RIL #58 rice plants. We performed punch inoculation assays using O23, TH3o, and d44a on RIL #58 (*Piks*) plants. (C) Quantification of the lesion size in (B). Statistically significant differences are indicated ($p < 0.01$, two-sided Welch's t-test).

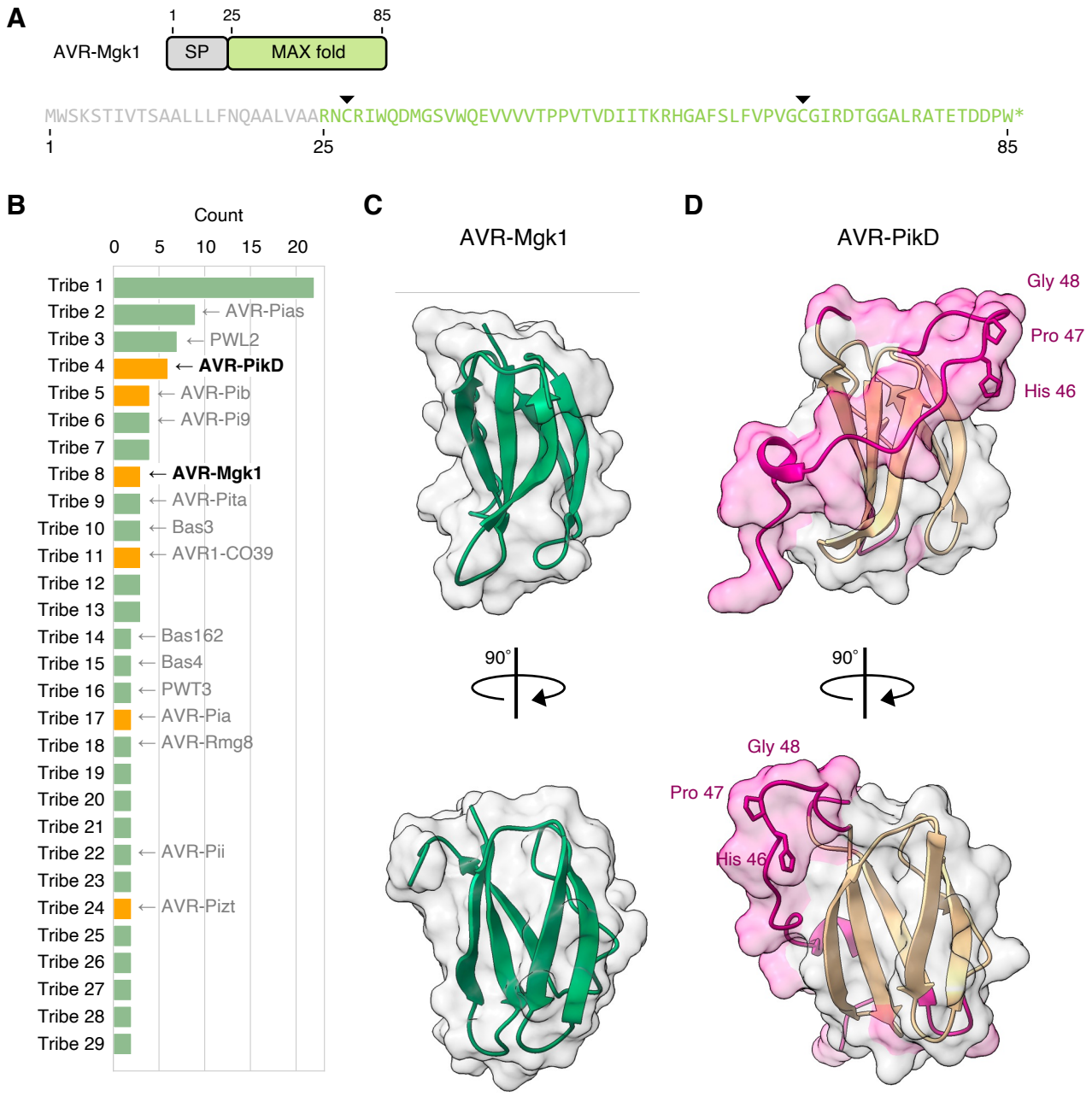

Fig. 6. AVR-Mgk1 is predicted to be a MAX fold protein that belongs to a distinct family from AVR-Pik effectors. (A) Domain architecture and amino acid sequence of AVR-Mgk1. We used SignalP v6.0 to predict signal peptide (SP) sequences in AVR-Mgk1. AVR-Mgk1 has the two cysteine residues (Cys27 and Cys67, indicated by black arrowheads) conserved in the MAX effector superfamily. (B) Clustering of putative *M. oryzae* AVR protein sequences using TRIBE-MCL [102]. Tribe-MCL assigned AVR-Mgk1 and AVR-PikD into different tribes. If a tribe includes an experimentally characterized protein, it is shown to represent the tribe. If a tribe includes an experimentally validated MAX effector protein or AVR-Mgk1, the tribe is shown in orange. Tribes having only one gene are not shown. (C) AVR-Mgk1 protein structure predicted by AlphaFold2 [103]. AVR-Mgk1 has antiparallel β sheets, characteristic of the MAX effector superfamily. (D) Protein structure of AVR-PikD (PDB ID: 6FU9 chain B) [70]. TM-align [104] revealed significant structural similarity between AVR-Mgk1 and AVR-PikD (**Fig. S10**), while the regions highlighted in pink structurally differ. This structural difference involves the highly polymorphic residues (His46-Pro47-Gly48) of AVR-Pik effectors that determine Pik-1 HMA domain binding and are probably modulated by arms race co-evolution [69,92].

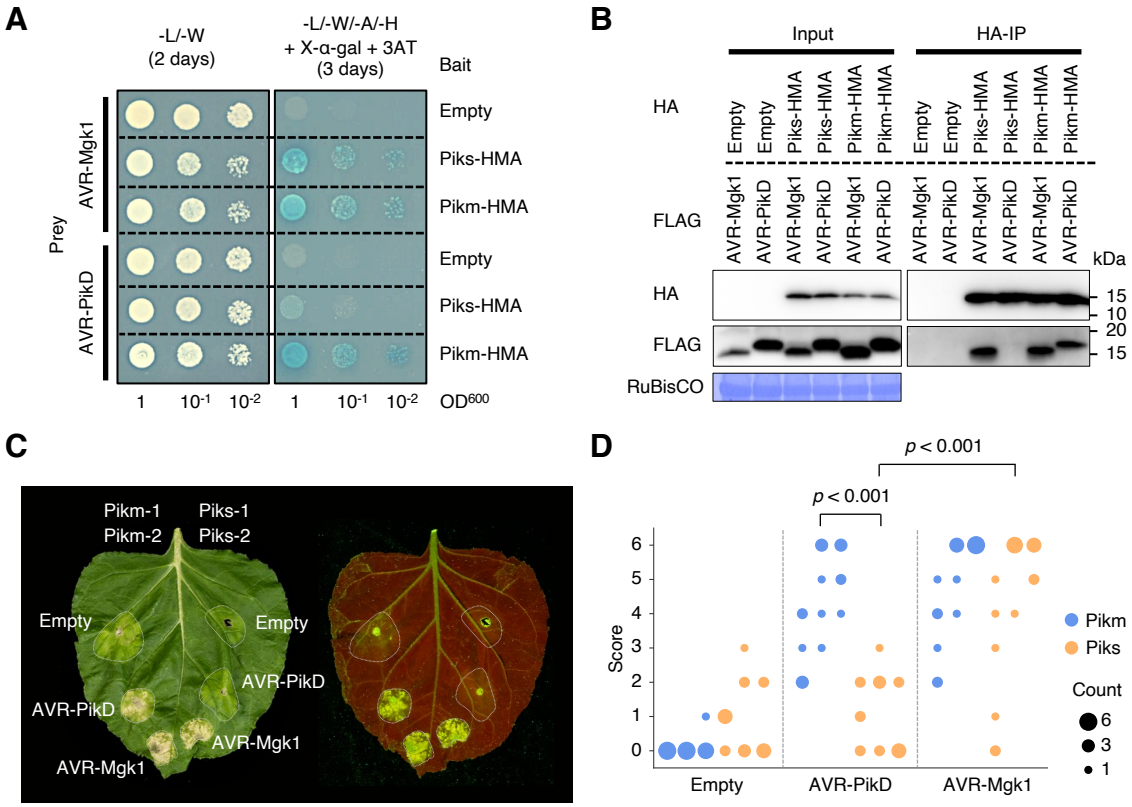

Fig. 7. Piks specifically responds to AVR-Mgk1 but not to AVR-PikD. (A) Yeast two-hybrid assays between the Pik integrated HMA domains and AVRs. We used Myc-tagged HMA domains and HA-tagged AVRs as bait and prey, respectively. Empty vector was used as a negative control. Left side: basal medium lacking leucine (L) and tryptophan (W) for growth control. Right side: basal medium lacking leucine (L), tryptophan (W), adenine (A), and histidine (H) and containing X-α-gal and 10 mM 3AT for selection. (B) *In vitro* co-immunoprecipitation (co-IP) experiments between the Pik integrated HMA domains and AVRs. We used N-terminally tagged HA:HMA and FLAG:AVR in the experiments, and the protein complexes were pulled down by HA:HMA using Anti-HA affinity gel. Empty vector was used as a negative control. The large subunit of ribulose bisphosphate carboxylase (RuBisCO) stained by Coomassie brilliant blue is shown as a loading control. (C) Representative images of hypersensitive response (HR) cell death assay after transient co-expression of the AVRs with Pik-1 and Pik-2 in *N. benthamiana*. Pikm and Piks were tested on the left and right sides of the leaf, respectively. The empty vector only expressing p19 was used as a negative control. The leaves were photographed 5–6 days after infiltration under daylight (left) and UV light (right). (D) The HR in (C) was quantified. Statistically significant differences are indicated (Mann-Whitney U rank test). Each column represents an independent experiment.

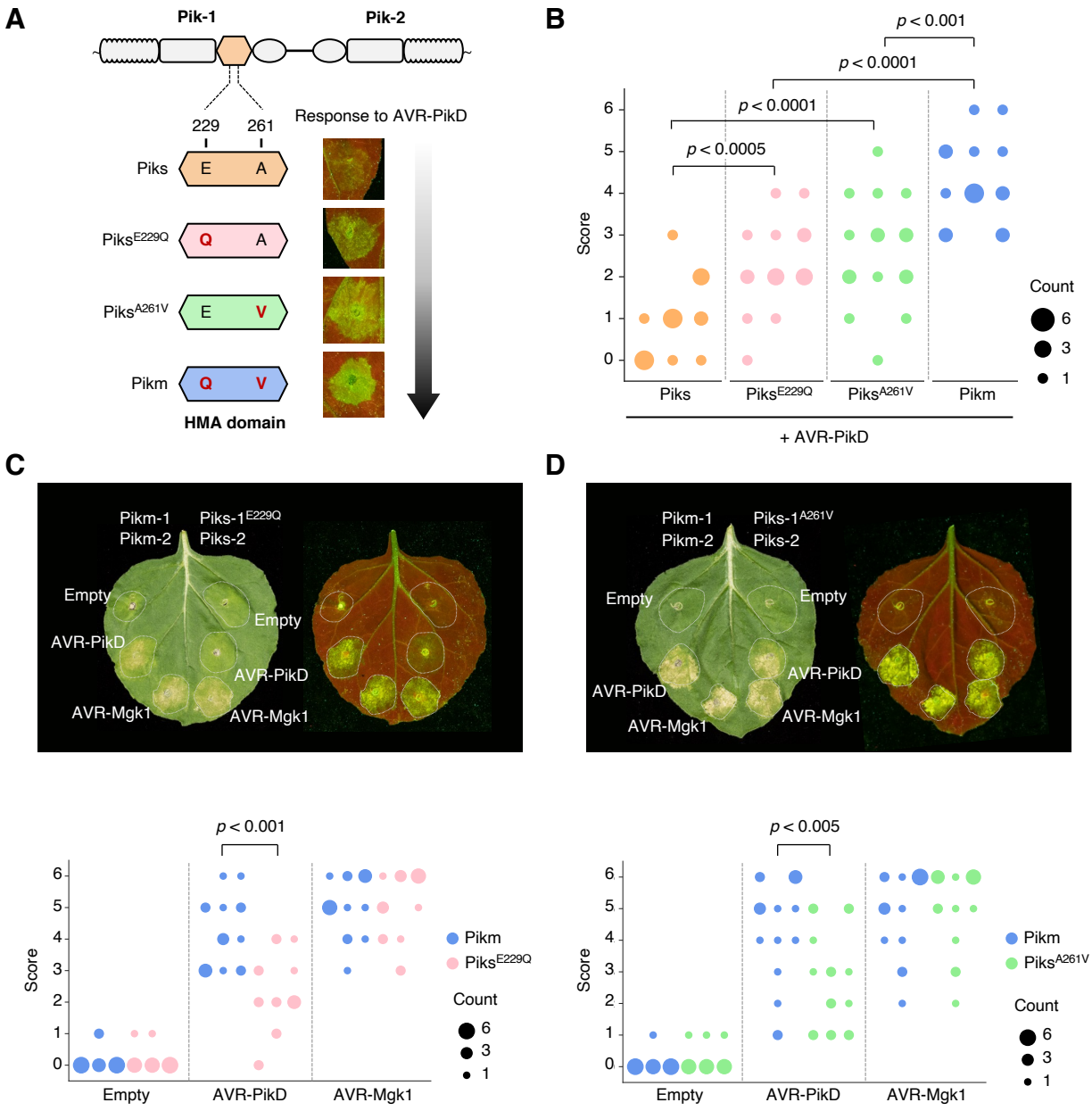

Fig. 8. The polymorphisms (E229Q and A261V) between Piks and Pikm quantitatively affect the response to AVR-PikD. (A) Schematic representations of single amino acid mutants (Piks^{E229Q} and Piks^{A261V}) used in the HR cell death assay in *N. benthamiana* with AVR-PikD. (B) We quantified HR scores of Piks (Piks-1/Piks-2), Piks^{E229Q} (Piks-1^{E229Q}/Piks-2), Piks^{A261V} (Piks-1^{A261V}/Piks-2), or Pikm (Pikm-1/Pikm-2) with AVR-PikD 5–6 days after agroinfiltration and statistically significant differences are indicated (Mann-Whitney U rank test). Piks-2 and Pikm-2 are identical. (C) HR cell death assay with Piks^{E229Q} and AVRs. (D) HR cell death assay with Piks^{A261V} and AVRs. The leaves were photographed 5–6 days after infiltration under daylight (left) and UV light (right). We quantified the HR at 5–6 days after agroinfiltration and statistically significant differences are indicated (Mann-Whitney U rank test). Each column represents an independent experiment.

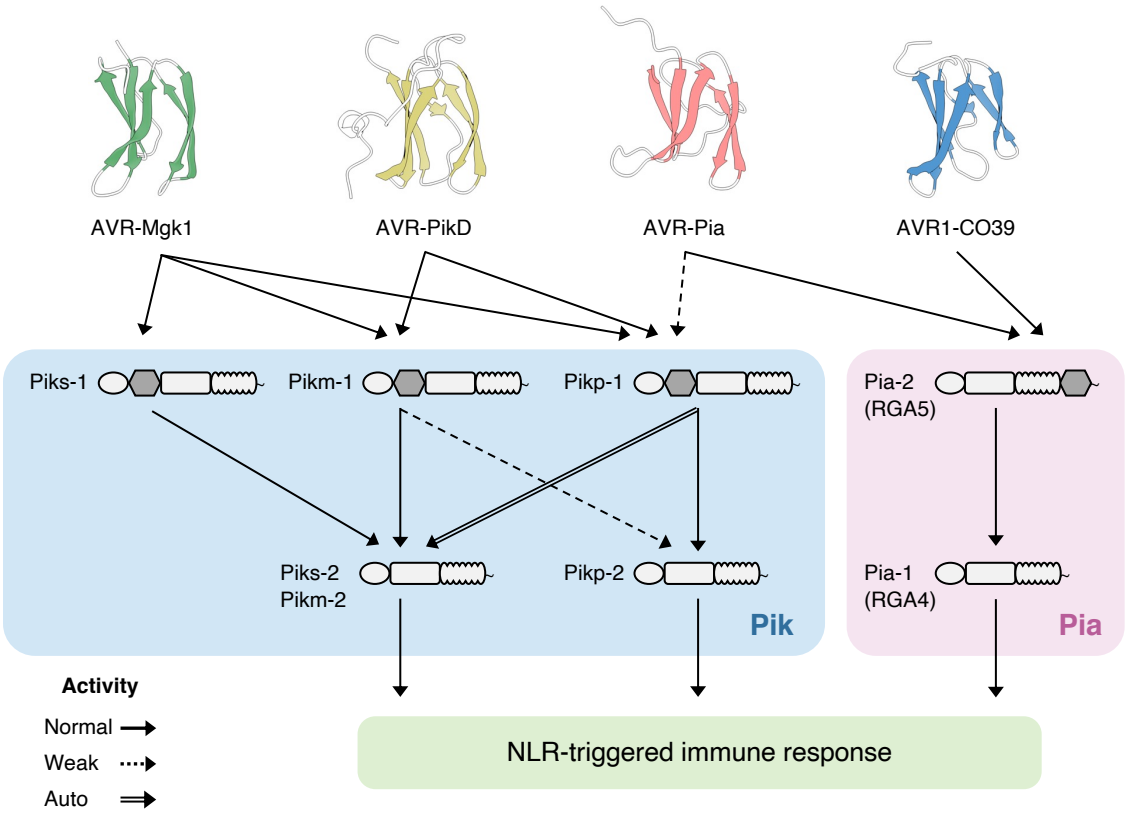

Fig. 9. Beyond the gene-for-gene model: complex interactions between MAX effectors and rice NLR pairs. The NLR pairs Pik (Pik-1/Pik-2) and Pia (Pia-2/Pia-1, also known as RGA5/RGA4) have an integrated HMA domain (grey) in their sensor NLRs (Pik-1 and Pia-2). The Pia-2 HMA domain binds the sequence-unrelated MAX effectors AVR-Pia and AVR1-CO39 [68]. The Pikp-1 HMA domain weakly binds AVR-Pia, while that of Pikm-1 cannot [111]. The AVR-Mgk1 effector is detected by several Pik proteins, including Piks, which does not respond to AVR-PikD. Complex interactions also occur between sensor and helper NLRs forming homo- and hetero-complexes [94,156]. An allelic mismatch of a receptor pair leads to autoimmunity (Pikp-1/Pikm-2) or reduced response (Pikm-1/Pikp-2) due to allelic specialization [157].The structures of AVR-Mgk1 predicted by AlphaFold2 [103], AVR-PikD (PDB ID: 6FU9 chain B) [70], AVR-Pia (PDB ID: 6Q76 chain B) [111], and AVR1-CO39 (PDB ID: 5ZNG chain C) [74] were visualised by ChimeraX [153].

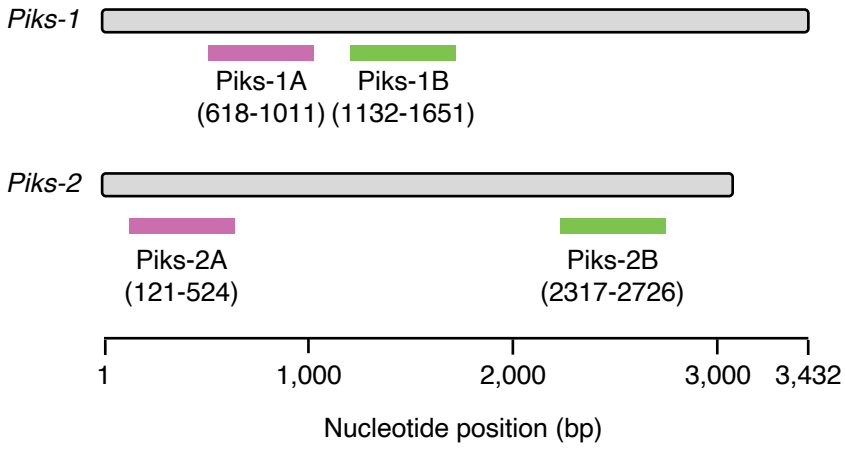

Fig. S1. Schematic representations of the RNAi-mediated *Pik-1* and *Pik-2* knockdown experiment. For each *Pik* gene, we prepared two independent RNAi constructs targeting different regions on the gene (Piks-1A and Piks-1B for *Piks-1*, and Piks-2A and Piks-2B for *Piks-2*).

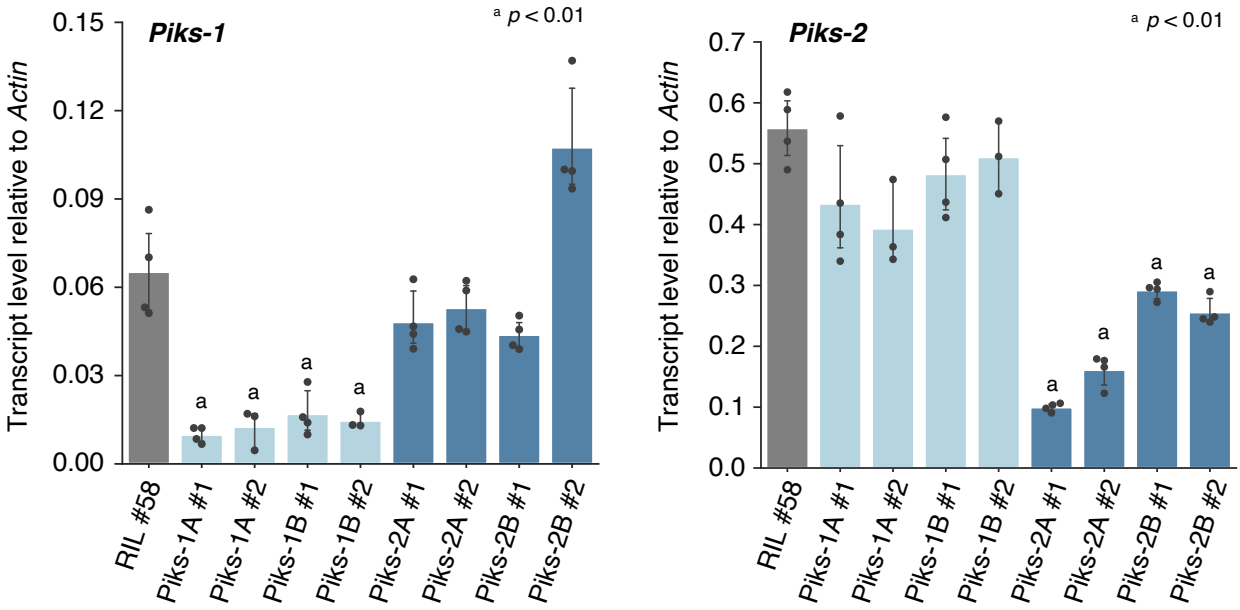

Fig. S2. *Piks-1* and *Piks-2* expression in RNAi-mediated knockdown lines. We analyzed *Piks-1* and *Piks-2* expression in RNAi-mediated knockdown lines using RT-qPCR. RIL #58 (*Pish* -, *Piks* +) was used as the genetic background for the mutant lines. Rice *Actin* was used for normalization. [a] indicates statistically significant differences compared to RIL #58 ($p < 0.01$, two-sided Welch's t-test).

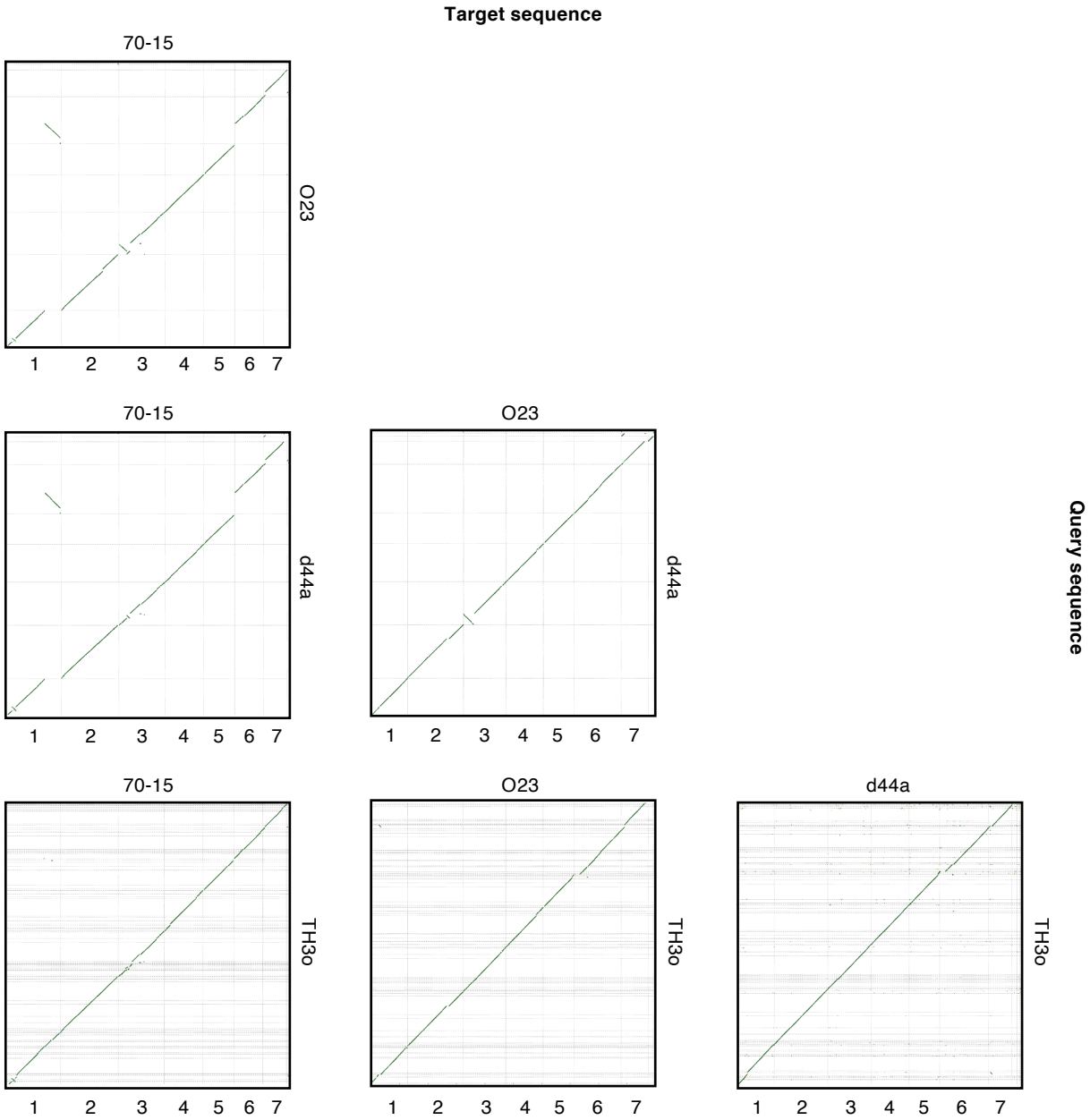

Fig. S3. Pairwise dot plot analyses among the *de novo*-assembled genome sequences of *M. oryzae* isolates 70-15, O23, TH3o, and d44a. We compared the *de novo*-assembled genome sequences of O23, TH3o, and d44a with the previously assembled reference genome (MG8 genome assembly) of the isolate 70-15 [96], using D-GENIES [139]. The chromosome sequences of O23 and d44a are numbered and ordered based on those of 70-15.

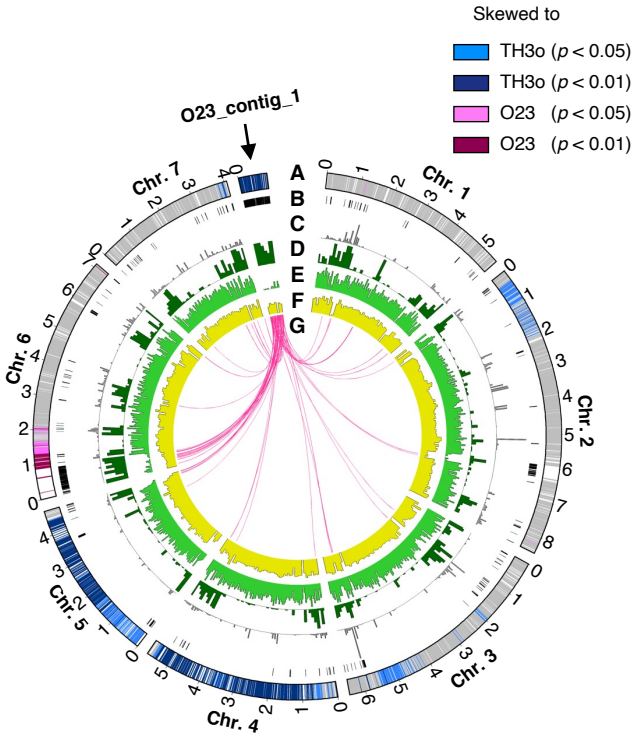

Fig. S4. Genomic features of a *M. oryzae* mini-chromosome O23_contig_1. (A) Segregation distortion in TH3o x O23 F_1 progeny. (B) O23-specific regions where TH3o contigs could not be aligned. (C) Recombination frequencies in the F_1 progeny. (D) Density of transposable elements. (E) Gene density. (F) GC contents (0.45–0.55). (G) Sequence similarity between the O23 mini-chromosome and core chromosomes (chromosomes 1–7).

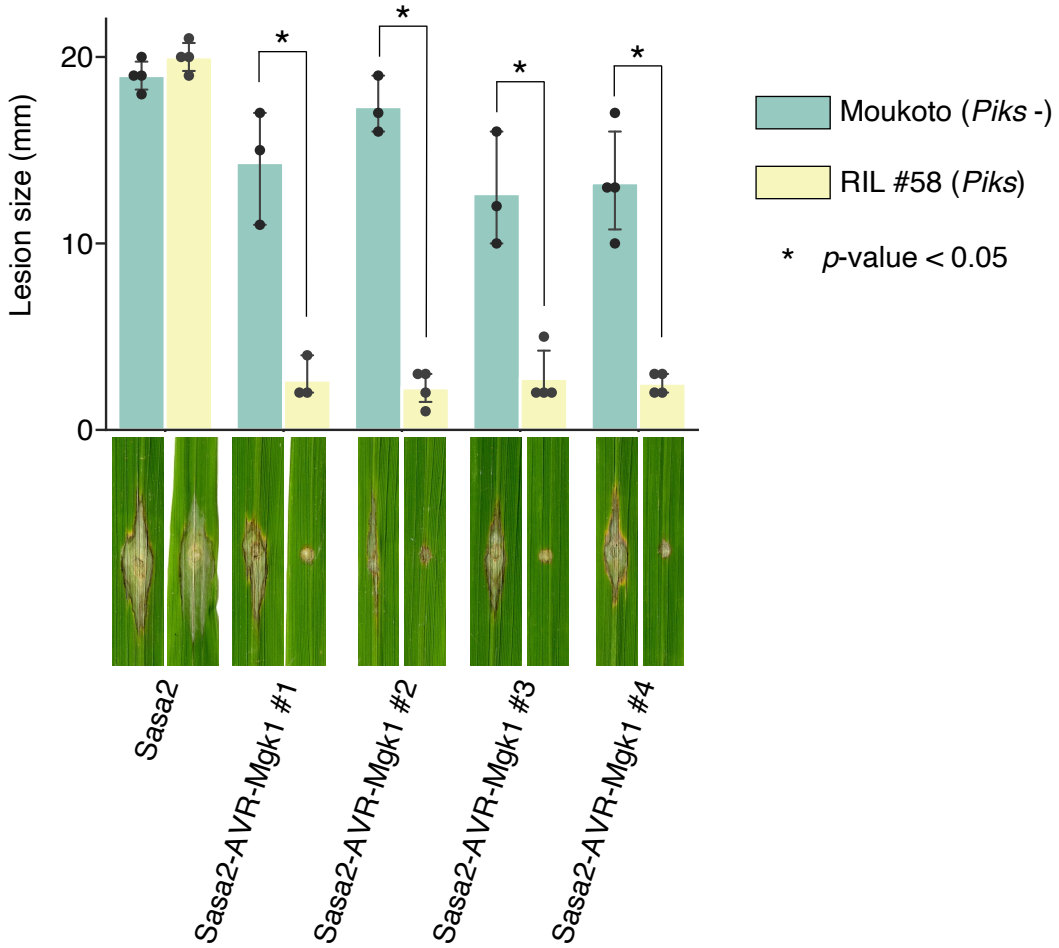

Fig. S5. Sasa2 transformants expressing *AVR-Mgk1* cannot infect RIL #58 rice plants containing *Piks*. We produced four independent *M. oryzae* Sasa2 transformants expressing *AVR-Mgk1* and performed punch inoculation assays using wild-type Sasa2 and Sasa2 transformants on rice lines Moukoto (*Piks* -) and RIL #58 (*Piks* +). The lesion size was quantified. Statistically significant differences between rice lines are indicated by asterisks ($p < 0.05$, two-sided Welch's t-test). The transformant Sasa2-AVR-Mgk1 #4 was used for the punch inoculation assay in Fig. 4D and 4E.

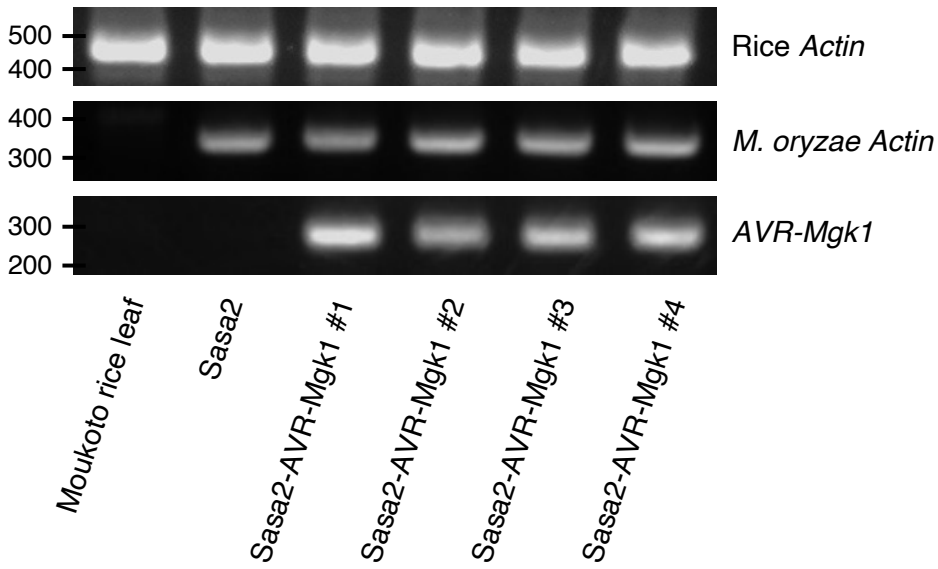

Fig. S6. *AVR-Mgk1* expression in infected rice leaves. We punch inoculated independent *M. oryzae* Sasa2 transformants expressing *AVR-Mgk1* on rice cultivar Moukoto. We reverse transcribed cDNA from RNA extracted from the infected rice leaves and amplified *AVR-Mgk1* via PCR. Rice and *M. oryzae Actin* were used as controls.

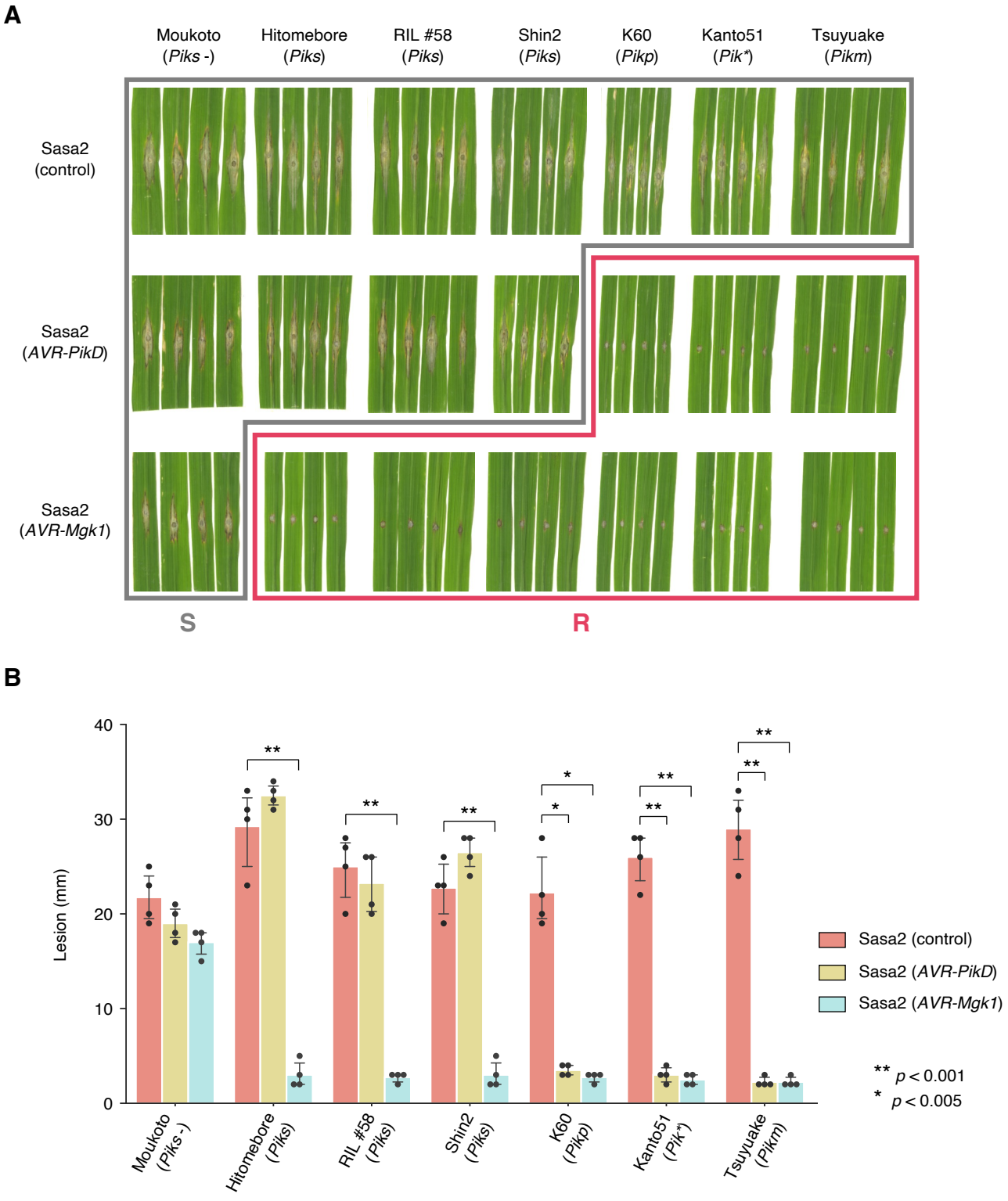

Fig. S7. Punch inoculation assays using Sasa2 transformants expressing *AVR-Mgk1* show the broad recognition of AVR-Mgk1 by Pik proteins. (A) We performed punch inoculation assays using wild-type Sasa2 and transformants expressing *AVR-PikD* and *AVR-Mgk1* on rice plants carrying different *Pik* alleles (*Piks*, *Pikp*, *Pik**, and *Pikm*). A subset of this picture was used in Fig. 4D. (B) The lesion size in (A) was quantified. Statistically significant differences between isolates are indicated by asterisks (two-sided Welch's t-test). A subset of this data was used in Fig. 4E.

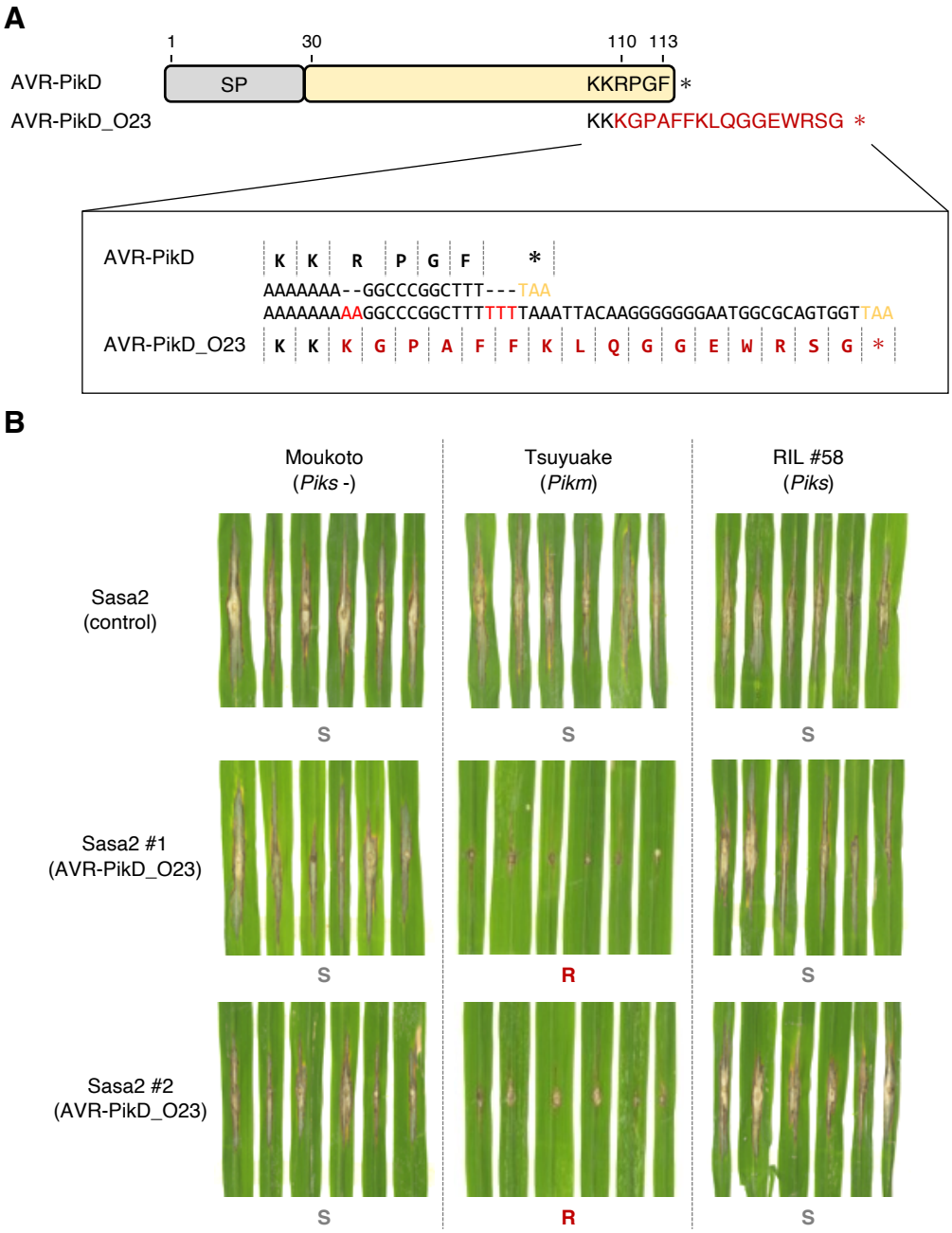

Fig. S8. The protein product of *AVR-PikD_O23*, carrying a frameshift mutation, is detected by Pikm but not by Piks. (A) *AVR-PikD* on the O23 mini-chromosome carries a frameshift mutation near the C-terminus that extends the amino acid sequence compared to previously described AVR-PikD. We named this variant *AVR-PikD_O23*. (B) Punch inoculation assays using Sasa2 and its transformant expressing *AVR-PikD_O23*. Sasa2 transformants expressing *AVR-PikD_O23* could not infect Tsuyuake (*Pikm*) but infected RIL #58 (*Piks*).

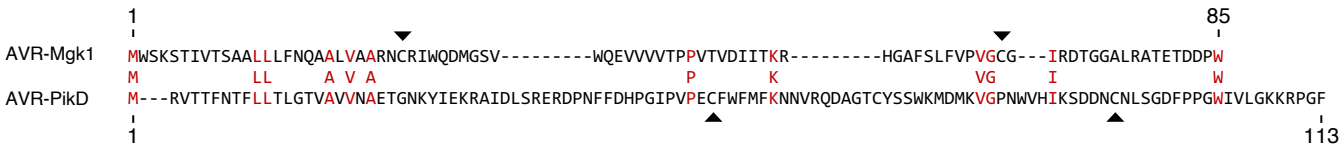

Fig. S9. Global sequence alignment reveals that AVR-Mgk1 and AVR-PikD are unrelated in amino acid sequence. We aligned the AVR-Mgk1 and AVR-PikD amino acid sequences using the Needleman-Wunsch global sequence alignment algorithm [150]. Twelve amino acids (red) are identical between AVR-Mgk1 and AVR-PikD. The two cysteine residues conserved in the MAX effector superfamily [27] are indicated by black arrowheads.

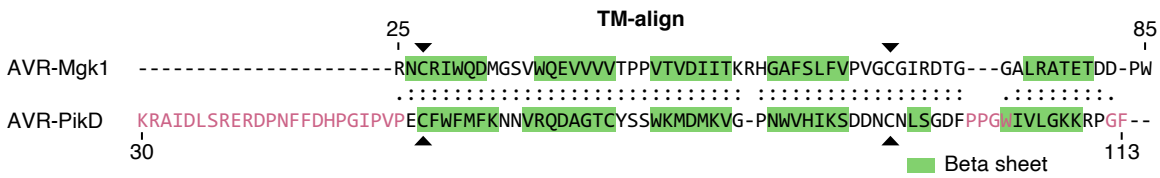

Fig. S10. Structure-based protein alignment reveals significant structural similarity between AVR-Mgk1 and AVR-PikD. We aligned the AVR-Mgk1 and AVR-PikD protein structures using TM-align [104]. TM-scores normalized by the sequence length of AVR-Mgk1 and AVR-PikD were 0.65 and 0.51, respectively, which indicates a similar fold [105]. The two cysteine residues conserved in the MAX effector superfamily [27] are indicated by black arrowheads. The pink regions in the AVR-PikD sequence indicate the structural differences between AVR-Mgk1 and AVR-PikD and correspond to the pink regions in Fig. 6D.

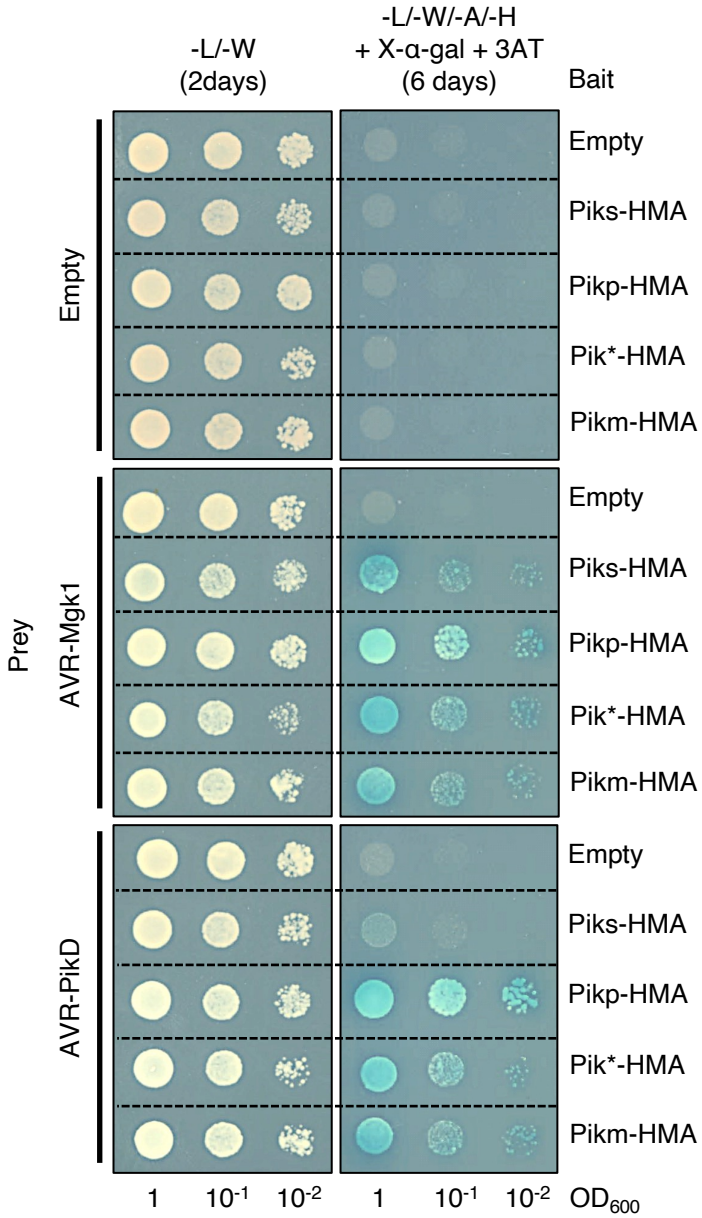

Fig. S11. Yeast two-hybrid assay shows that the HMA domains of Pik proteins (bait) bind AVR-Mgk1 (prey). We used HA-tagged AVRs as prey and Myc-tagged HMA domains as bait. Empty vector was used as a negative control. Left side: basal medium lacking leucine (L) and tryptophan (W) for growth control. Right side: basal medium lacking leucine (L), tryptophan (W), adenine (A), and histidine (H) and containing X-α-gal and 10 mM 3AT for selection.

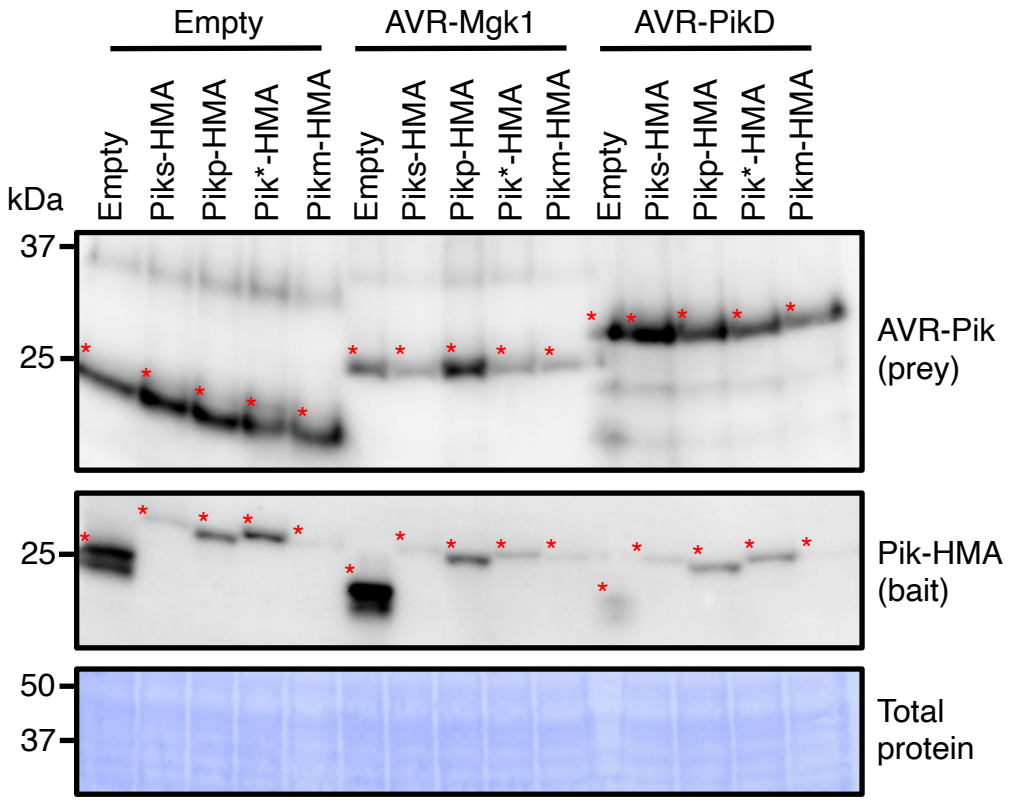

Fig. S12. Accumulation of AVRs (prey) and HMA domains (bait) in yeast cells as confirmed by immunoblot analysis. To confirm protein accumulation for the yeast two-hybrid assay, we detected HA-tagged AVRs (prey) by anti-HA antibody and Myc-tagged HMA domains (bait) by anti-Myc antibody. Total proteins of yeast cells detected by Coomassie brilliant blue staining are shown in the bottom as a loading control.

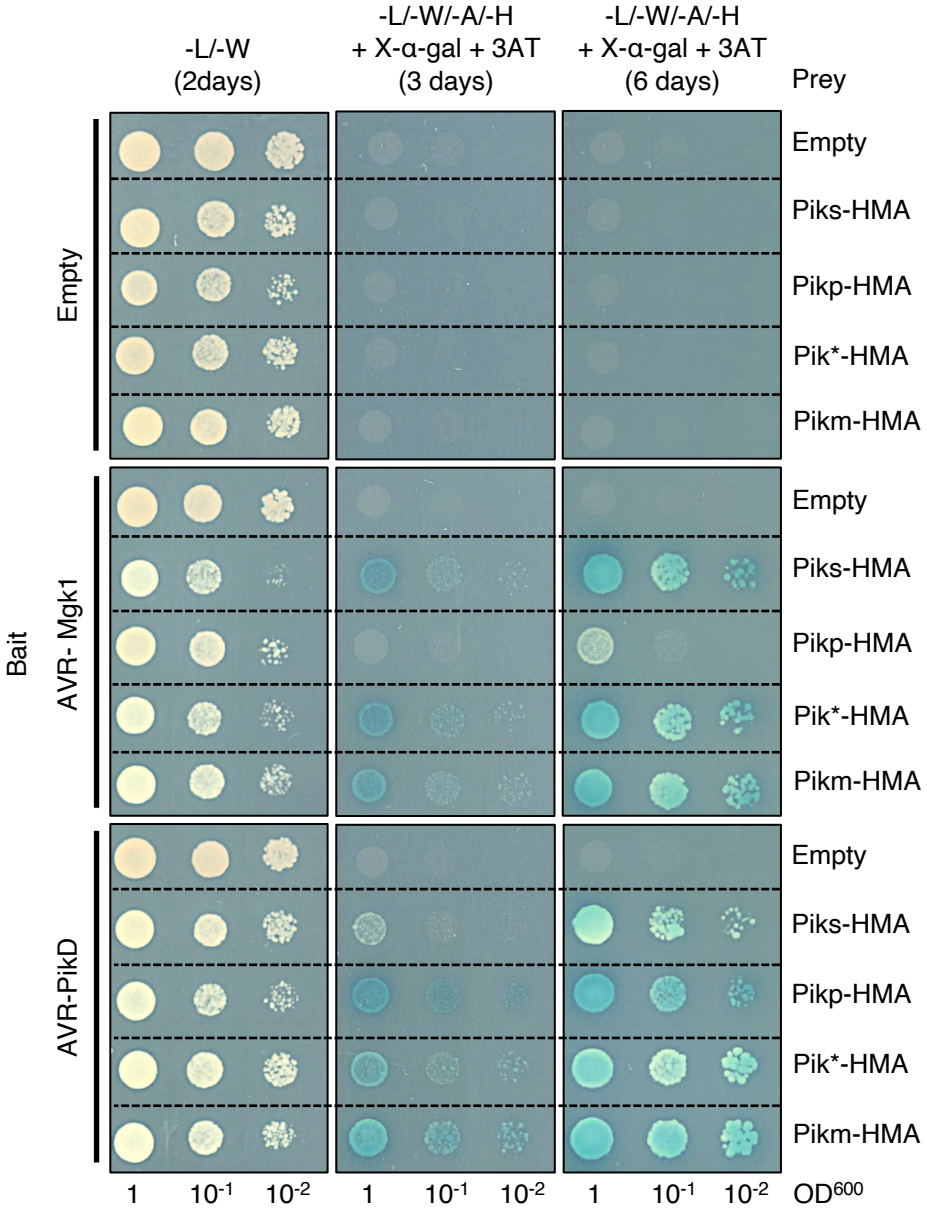

Fig. S13. Yeast two-hybrid assay shows that the HMA domains of Pik proteins (prey) bind AVR-Mgk1 (bait). We used Myc-tagged AVRs as bait and HA-tagged HMA domains as prey. Empty vector was used as a negative control. Left side: basal medium lacking leucine (L) and tryptophan (W) for growth control. Right side: basal medium lacking leucine (L), tryptophan (W), adenine (A), and histidine (H) and containing X-α-gal and 10 mM 3AT for selection.

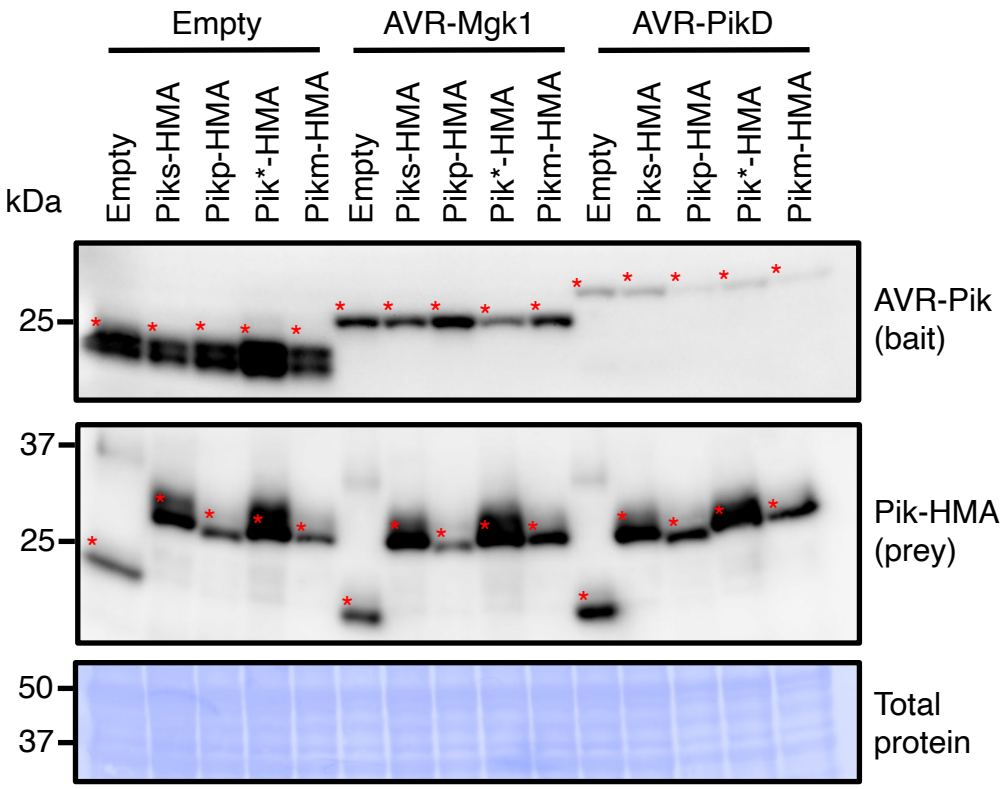

Fig. S14. Accumulation of AVRs (bait) and HMA domains (prey) in yeast cells as confirmed by immunoblot analysis. To confirm protein accumulation for the yeast two-hybrid assay, we detected Myc-tagged AVRs (bait) by anti-Myc antibody and HA-tagged HMA domains (prey) by anti-HA antibody. Total proteins of yeast cells detected by Coomassie brilliant blue staining are shown in the bottom as a loading control.

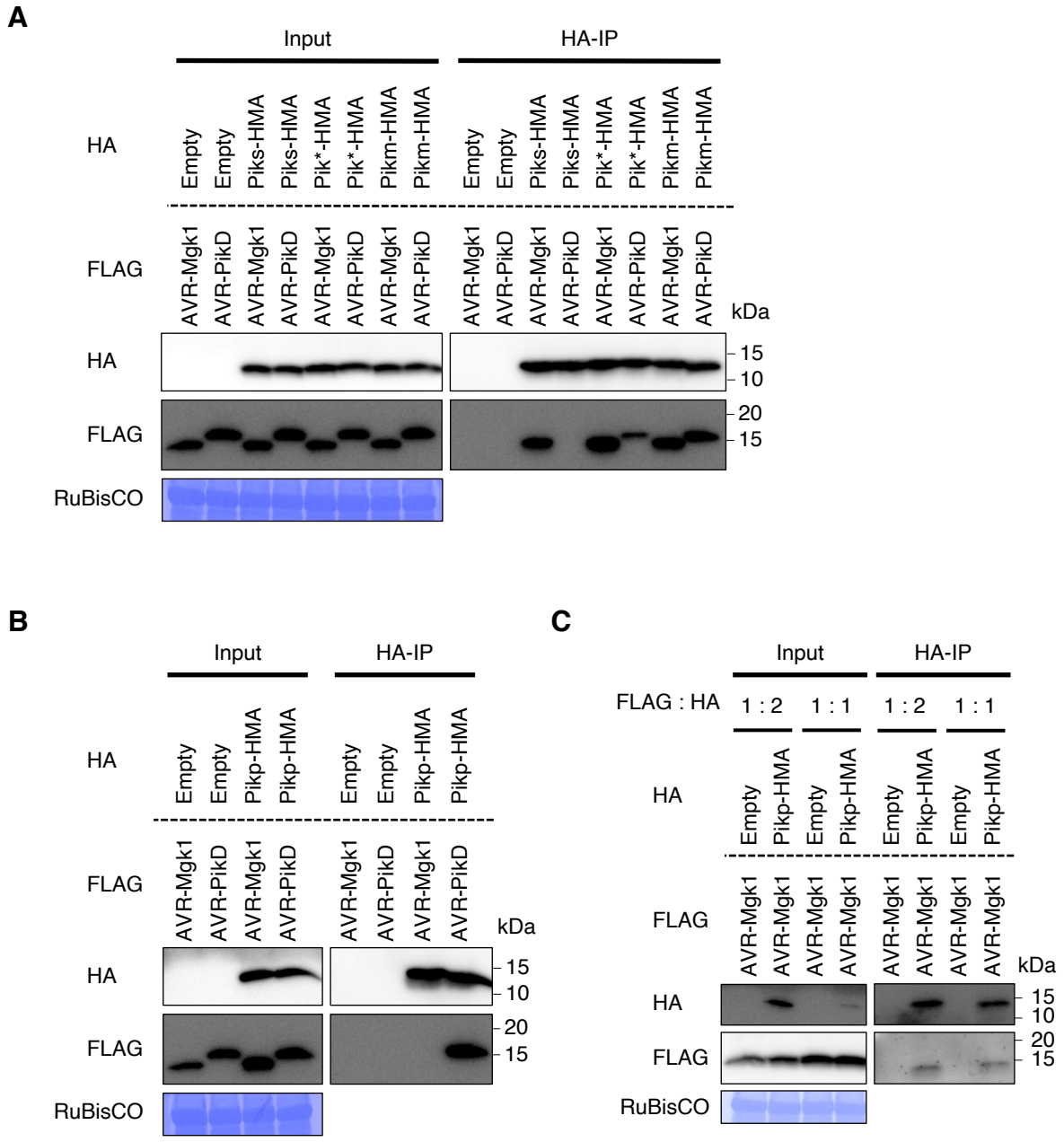

Fig. S15. AVR-Mgk1 interacts with the HMA domains of Pik proteins in an *in vitro* co-IP experiment. (A) *In vitro* co-IP experiment between AVR-Mgk1 or AVR-PikD and the HMA domains of Piks (Piks-HMA), Pikm (Pikm-HMA), or Pik* (Pik*-HMA) (1:4 mixed ratio). (B) *In vitro* co-IP experiment between AVR-Mgk1 or AVR-PikD and the HMA domain of Pikp (Pikp-HMA) (1:4 mixed ratio). (C) *In vitro* co-IP experiment between AVR-Mgk1 and Pikp-HMA (1:2 or 1:1 mixed ratios). N-terminally tagged FLAG:AVRs and HA:HMA were expressed in *N. benthamiana*. Empty vector was used as a negative control. We diluted the lysates of AVRs and HMA domains to compare the results at the same concentration and mixed them (1:4, 1:2, or 1:1 ratio) *in vitro* to assemble the protein complex. The protein complexes were pulled down by HA:HMA using Anti-HA affinity gel. *In vitro* co-IP experiments between AVR-Mgk1 and Pikp-HMA (1:2 or 1:1 mixed ratios) were photographed in long-exposure time. The large subunit of ribulose bisphosphate carboxylase (RuBisCO) stained by Coomassie brilliant blue is shown as a loading control.

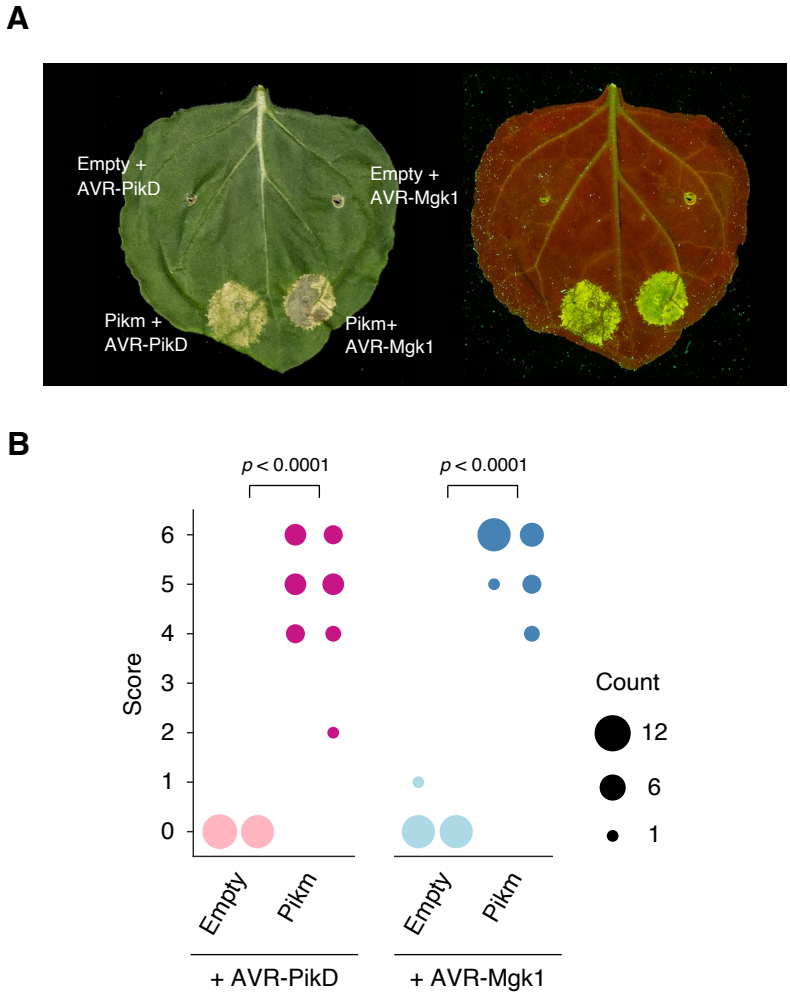

Fig. S16. AVR-Mgk1 and AVR-PikD alone do not trigger the HR in *N. benthamiana*. (A) Representative images 5–6 days after transiently co-expressing AVR-Mgk1 and AVR-PikD, either with an empty vector control only expressing p19 or with Pikm, respectively, in *N. benthamiana*. The leaves were photographed under daylight (left) and UV light (right). (B) We quantified the HR in (A) and statistically significant differences are indicated (Mann-Whitney U rank test). Each column shows an independent experiment.

Supplementary tables

Table S1. Summary of sequences of rice cultivars Hitomebore and Moukoto and their RILs.

Table S2. Summary of phenotypes of rice RILs derived from a cross between Hitomebore and Moukoto.

Table S3. Summary of *de novo* assemblies of the *M. oryzae* isolates TH3, O23, and d44a.

Table S4. Summary of sequences of *M. oryzae* isolates TH3o and O23 and their F_1 progeny.

Table S5. Summary of infectivity of the TH3o x O23 F_1 progeny on RIL #58 and Moukoto rice plants.

Table S6. BLAST search results using AVR-Mgk1 as query.

Table S7. Summary of the various interactions and phenotypes between Pik NLRs and AVRs in this study.

Table S8. Primer sequences used in this study.

Table S9. Cloning details of constructs used for the hypersensitive response cell death assays.

References

1. Flor HH. Current Status of the Gene-For-Gene Concept. Annu Rev Phytopathol. 1971;9: 275–296. doi:10.1146/annurev.py.09.090171.001423

2. Wu C-H, Derevnina L, Kamoun S. Receptor networks underpin plant immunity. Science. 2018;360: 1300–1301. doi:10.1126/science.aat2623

3. Derevnina L, Contreras MP, Adachi H, Upson J, Cruces AV, Xie R, et al. Plant pathogens convergently evolved to counteract redundant nodes of an NLR immune receptor network. PLOS Biol. 2021;19: e3001136. doi:10.1371/journal.pbio.3001136

4. Petit-Houdenot Y, Fudal I. Complex Interactions between Fungal Avirulence Genes and Their Corresponding Plant Resistance Genes and Consequences for Disease Resistance Management. Front Plant Sci. 2017;8. doi:10.3389/fpls.2016.00241

5. Bourras S, McNally KE, Müller MC, Wicker T, Keller B. Avirulence Genes in Cereal Powdery Mildews: The Gene-for-Gene Hypothesis 2.0. Front Plant Sci. 2016;7. doi:10.3389/fpls.2016.00241

6. Dean R, Van Kan J a. L, Pretorius ZA, Hammond-Kosack KE, Di Pietro A, Spanu PD, et al. The Top 10 fungal pathogens in molecular plant pathology. Mol Plant Pathol. 2012;13: 414–430. doi:10.1111/j.1364-3703.2011.00783.x

7. Gladieux P, Condon B, Ravel S, Soanes D, Maciel JLN, Nhani A, et al. Gene Flow between Divergent Cereal- and Grass-Specific Lineages of the Rice Blast Fungus Magnaporthe oryzae. Taylor JW, editor. mBio. 2018;9: e01219-17. doi:10.1128/mBio.01219-17

8. Tosa Y, Osue J, Eto Y, Oh H-S, Nakayashiki H, Mayama S, et al. Evolution of an Avirulence Gene, AVR1-CO39, Concomitant with the Evolution and Differentiation of Magnaporthe oryzae. Mol Plant-Microbe Interactions. 2005;18: 1148–1160. doi:10.1094/MPMI-18-1148

9. Chiapello H, Mallet L, Guérin C, Aguileta G, Amselem J, Kroj T, et al. Deciphering Genome Content and Evolutionary Relationships of Isolates from the Fungus Magnaporthe oryzae Attacking Different Host Plants. Genome Biol Evol. 2015;7: 2896–2912. doi:10.1093/gbe/evv187

10. Yoshida K, Saunders DGO, Mitsuoka C, Natsume S, Kosugi S, Saitoh H, et al. Host specialization of the blast fungus Magnaporthe oryzae is associated with dynamic gain and loss of genes linked to transposable elements. BMC Genomics. 2016;17: 370. doi:10.1186/s12864-016-2690-6

11. Inoue Y, Vy TTP, Yoshida K, Asano H, Mitsuoka C, Asuke S, et al. Evolution of the wheat blast fungus through functional losses in a host specificity determinant. Science. 2017;357: 80–83. doi:10.1126/science.aam9654

12. Franceschetti M, Maqbool A, Jiménez-Dalmaroni MJ, Pennington HG, Kamoun S, Banfield MJ. Effectors of Filamentous Plant Pathogens: Commonalities amid Diversity. Microbiol Mol Biol Rev. 2017;81: e00066-16. doi:10.1128/MMBR.00066-16

13. Kang S, Sweigard JA, Valent B. The PWL host specificity gene family in the blast fungus Magnaporthe grisea. Mol Plant-Microbe Interactions. 1995;8: 939–948.

14. Sweigard JA, Carroll AM, Kang S, Farrall L, Chumley FG, Valent B. Identification, cloning, and characterization of PWL2, a gene for host species specificity in the rice blast fungus. Plant Cell. 1995;7: 1221–1233.

15. Orbach MJ, Farrall L, Sweigard JA, Chumley FG, Valent B. A Telomeric Avirulence Gene Determines Efficacy for the Rice Blast Resistance Gene Pi-ta. Plant Cell. 2000;12: 2019–2032. doi:10.1105/tpc.12.11.2019

16. Miki S, Matsui K, Kito H, Otsuka K, Ashizawa T, Yasuda N, et al. Molecular cloning and characterization of the AVR-Pia locus from a Japanese field isolate of Magnaporthe oryzae. Mol Plant Pathol. 2009;10: 361–374. doi:10.1111/j.1364-3703.2009.00534.x

17. Yoshida K, Saitoh H, Fujisawa S, Kanzaki H, Matsumura H, Yoshida K, et al. Association Genetics Reveals Three Novel Avirulence Genes from the Rice Blast Fungal Pathogen Magnaporthe oryzae. Plant Cell. 2009;21: 1573–1591. doi:10.1105/tpc.109.066324

18. Farman ML, Leong SA. Chromosome Walking to the AVR1-CO39 Avirulence Gene of Magnaporthe grisea: Discrepancy Between the Physical and Genetic Maps. Genetics. 1998;150: 1049–1058. doi:10.1093/genetics/150.3.1049

19. Ribot C, Césari S, Abidi I, Chalvon V, Bournaud C, Vallet J, et al. The Magnaporthe oryzae effector AVR1–CO39 is translocated into rice cells independently of a fungal-derived machinery. Plant J. 2013;74: 1–12. doi:10.1111/tpj.12099

20. Li W, Wang B, Wu J, Lu G, Hu Y, Zhang X, et al. The Magnaporthe oryzae Avirulence Gene AvrPiz-t Encodes a Predicted Secreted Protein That Triggers the Immunity in Rice Mediated by the Blast Resistance Gene Piz-t. Mol Plant-Microbe Interactions. 2009;22: 411–420. doi:10.1094/MPMI-22-4-0411

21. Wu J, Kou Y, Bao J, Li Y, Tang M, Zhu X, et al. Comparative genomics identifies the Magnaporthe oryzae avirulence effector AvrPi9 that triggers Pi9-mediated blast resistance in rice. New Phytol. 2015;206: 1463–1475. doi:10.1111/nph.13310

22. Zhang S, Wang L, Wu W, He L, Yang X, Pan Q. Function and evolution of Magnaporthe oryzae avirulence gene AvrPib responding to the rice blast resistance gene Pib. Sci Rep. 2015;5: 11642. doi:10.1038/srep11642

23. Ray S, Singh PK, Gupta DK, Mahato AK, Sarkar C, Rathour R, et al. Analysis of Magnaporthe oryzae Genome Reveals a Fungal Effector, Which Is Able to Induce Resistance Response in Transgenic Rice Line Containing Resistance Gene, Pi54. Front Plant Sci. 2016;7: 1140. doi:10.3389/fpls.2016.01140

24. Anh VL, Inoue Y, Asuke S, Vy TTP, Anh NT, Wang S, et al. Rmg8 and Rmg7, wheat genes for resistance to the wheat blast fungus, recognize the same avirulence gene AVR-Rmg8. Mol Plant Pathol. 2018;19: 1252–1256. doi:10.1111/mpp.12609

25. Shimizu M, Hirabuchi A, Sugihara Y, Abe A, Takeda T, Kobayashi M, et al. A genetically linked pair of NLR immune receptors shows contrasting patterns of evolution. Proc Natl Acad Sci. 2022;119: e2116896119. doi:10.1073/pnas.2116896119

26. Zhang Z-M, Zhang X, Zhou Z-R, Hu H-Y, Liu M, Zhou B, et al. Solution structure of the Magnaporthe oryzae avirulence protein AvrPiz-t. J Biomol NMR. 2013;55: 219–223. doi:10.1007/s10858-012-9695-5

27. de Guillen K, Ortiz-Vallejo D, Gracy J, Fournier E, Kroj T, Padilla A. Structure Analysis Uncovers a Highly Diverse but Structurally Conserved Effector Family in Phytopathogenic Fungi. PLOS Pathog. 2015;11: e1005228. doi:10.1371/journal.ppat.1005228

28. Maqbool A, Saitoh H, Franceschetti M, Stevenson C, Uemura A, Kanzaki H, et al. Structural basis of pathogen recognition by an integrated HMA domain in a plant NLR immune receptor. Nürnberger T, editor. eLife. 2015;4: e08709. doi:10.7554/eLife.08709

29. Zhang X, He D, Zhao Y, Cheng X, Zhao W, Taylor IA, et al. A positive-charged patch and stabilized hydrophobic core are essential for avirulence function of AvrPib in the rice blast fungus. Plant J. 2018;96: 133–146. doi:10.1111/tpj.14023

30. De la Concepcion JC, Fujisaki K, Bentham AR, Mireles NC, de Medina Hernandez VS, Shimizu M, et al. Binding of a blast fungus Zinc-finger fold effector to a hydrophobic pocket in the host exocyst subunit Exo70 modulates immune recognition in rice. bioRxiv; 2022 Jun. doi:10.1101/2022.06.18.496527

31. Petit-Houdenot Y, Langner T, Harant A, Win J, Kamoun S. A Clone Resource of Magnaporthe oryzae Effectors That Share Sequence and Structural Similarities Across Host-Specific Lineages. Mol Plant-Microbe Interactions. 2020;33: 1032–1035. doi:10.1094/MPMI-03-20-0052-A

32. Bentham AR, Petit-Houdenot Y, Win J, Chuma I, Terauchi R, Banfield MJ, et al. A single amino acid polymorphism in a conserved effector of the multihost blast fungus pathogen expands host-target binding spectrum. PLOS Pathog. 2021;17: e1009957. doi:10.1371/journal.ppat.1009957

33. Seong K, Krasileva K. Comparative computational structural genomics highlights divergent evolution of fungal effectors. bioRxiv; 2022. p. 2022.05.02.490317. doi:10.1101/2022.05.02.490317

34. Seong K, Krasileva KV. Computational Structural Genomics Unravels Common Folds and Novel Families in the Secretome of Fungal Phytopathogen Magnaporthe oryzae. Mol Plant-Microbe Interactions. 2021;34: 1267–1280. doi:10.1094/MPMI-03-21-0071-R

35. Ma L-J, van der Does HC, Borkovich KA, Coleman JJ, Daboussi M-J, Di Pietro A, et al. Comparative genomics reveals mobile pathogenicity chromosomes in Fusarium. Nature. 2010;464: 367–373. doi:10.1038/nature08850

36. Stukenbrock EH, Jørgensen FG, Zala M, Hansen TT, McDonald BA, Schierup MH. Whole-Genome and Chromosome Evolution Associated with Host Adaptation and Speciation of the Wheat Pathogen Mycosphaerella graminicola. PLOS Genet. 2010;6: e1001189. doi:10.1371/journal.pgen.1001189

37. Goodwin SB, M'Barek SB, Dhillon B, Wittenberg AHJ, Crane CF, Hane JK, et al. Finished Genome of the Fungal Wheat Pathogen Mycosphaerella graminicola Reveals Dispensome Structure, Chromosome Plasticity, and Stealth Pathogenesis. PLOS Genet. 2011;7: e1002070. doi:10.1371/journal.pgen.1002070

38. Croll D, Zala M, McDonald BA. Breakage-fusion-bridge Cycles and Large Insertions Contribute to the Rapid Evolution of Accessory Chromosomes in a Fungal Pathogen. PLOS Genet. 2013;9: e1003567. doi:10.1371/journal.pgen.1003567

39. Croll D, McDonald BA. The Accessory Genome as a Cradle for Adaptive Evolution in Pathogens. PLOS Pathog. 2012;8: e1002608. doi:10.1371/journal.ppat.1002608

40. Jones N. New species with B chromosomes discovered since 1980. The Nucleus. 2017;60: 263–281. doi:10.1007/s13237-017-0215-6

41. Talbot NJ, Salch YP, Ma M, Hamer JE. Karyotypic Variation within Clonal Lineages of the Rice Blast Fungus, Magnaporthe grisea. Appl Environ Microbiol. 1993;59: 585–593. doi:10.1128/aem.59.2.585-593.1993

42. Orbach MJ, Chumley FG, Valent B. Electrophoretic karyotypes of Magnaporthe grisea pathogens of diverse grasses. Mol Plant-Microbe Interactions. 1996;9: 261–271.

43. Mills D, McCluskey K. Electrophoretic karyotypes of fungi: the new cytology. Mol Plant Microbe Interact. 1990;3: 351–357.

44. Peng Z, Oliveira-Garcia E, Lin G, Hu Y, Dalby M, Migeon P, et al. Effector gene reshuffling involves dispensable mini-chromosomes in the wheat blast fungus. PLOS Genet. 2019;15: e1008272. doi:10.1371/journal.pgen.1008272

45. Langner T, Harant A, Gomez-Luciano LB, Shrestha RK, Malmgren A, Latorre SM, et al. Genomic rearrangements generate hypervariable mini-chromosomes in host-specific isolates of the blast fungus. PLOS Genet. 2021;17: e1009386. doi:10.1371/journal.pgen.1009386

46. Chuma I, Isobe C, Hotta Y, Ibaragi K, Futamata N, Kusaba M, et al. Multiple Translocation of the AVR-Pita Effector Gene among Chromosomes of the Rice Blast Fungus Magnaporthe oryzae and Related Species. PLOS Pathog. 2011;7: e1002147. doi:10.1371/journal.ppat.1002147

47. Luo C-X, Yin L-F, Ohtaka K, Kusaba M. The 1.6Mb chromosome carrying the avirulence gene AvrPik in Magnaporthe oryzae isolate 84R-62B is a chimera containing chromosome 1 sequences. Mycol Res. 2007;111: 232–239. doi:10.1016/j.mycres.2006.10.008

48. Kusaba M, Mochida T, Naridomi T, Fujita Y, Chuma I, Tosa Y. Loss of a 1.6 Mb chromosome in Pyricularia oryzae harboring two alleles of AvrPik leads to acquisition of virulence to rice cultivars containing resistance alleles at the Pik locus. Curr Genet. 2014;60: 315–325. doi:10.1007/s00294-014-0437-y

49. Böhnert HU, Fudal I, Dioh W, Tharreau D, Notteghem J-L, Lebrun M-H. A Putative Polyketide Synthase/Peptide Synthetase from Magnaporthe grisea Signals Pathogen Attack to Resistant Rice. Plant Cell. 2004;16: 2499–2513. doi:10.1105/tpc.104.022715

50. Mosquera G, Giraldo MC, Khang CH, Coughlan S, Valent B. Interaction Transcriptome Analysis Identifies Magnaporthe oryzae BAS1-4 as Biotrophy-Associated Secreted Proteins in Rice Blast Disease. Plant Cell. 2009;21: 1273–1290. doi:10.1105/tpc.107.055228

51. Ma L-J, Xu J-R. Shuffling effector genes through mini-chromosomes. PLOS Genet. 2019;15: e1008345. doi:10.1371/journal.pgen.1008345

52. Kourelis J, van der Hoorn RAL. Defended to the Nines: 25 Years of Resistance Gene Cloning Identifies Nine Mechanisms for R Protein Function. Plant Cell. 2018;30: 285–299. doi:10.1105/tpc.17.00579

53. Adachi H, Derevnina L, Kamoun S. NLR singletons, pairs, and networks: evolution, assembly, and regulation of the intracellular immunoreceptor circuitry of plants. Curr Opin Plant Biol. 2019;50: 121–131. doi:10.1016/j.pbi.2019.04.007

54. Araújo AC de, Fonseca FCDA, Cotta MG, Alves GSC, Miller RNG. Plant NLR receptor proteins and their potential in the development of durable genetic resistance to biotic stresses. Biotechnol Res Innov. 2019;3: 80–94. doi:10.1016/j.biori.2020.01.002

55. Takken FL, Goverse A. How to build a pathogen detector: structural basis of NB-LRR function. Curr Opin Plant Biol. 2012;15: 375–384. doi:10.1016/j.pbi.2012.05.001

56. Shao Z-Q, Xue J-Y, Wu P, Zhang Y-M, Wu Y, Hang Y-Y, et al. Large-Scale Analyses of Angiosperm Nucleotide-Binding Site-Leucine-Rich Repeat Genes Reveal Three Anciently Diverged Classes with Distinct Evolutionary Patterns. Plant Physiol. 2016;170: 2095–2109. doi:10.1104/pp.15.01487

57. Shao Z-Q, Xue J-Y, Wang Q, Wang B, Chen J-Q. Revisiting the Origin of Plant NBS-LRR Genes. Trends Plant Sci. 2019;24: 9–12. doi:10.1016/j.tplants.2018.10.015

58. Kourelis J, Sakai T, Adachi H, Kamoun S. RefPlantNLR is a comprehensive collection of experimentally validated plant disease resistance proteins from the NLR family. PLOS Biol. 2021;19: e3001124. doi:10.1371/journal.pbio.3001124

59. Barragan AC, Weigel D. Plant NLR diversity: the known unknowns of pan-NLRomes. Plant Cell. 2021;33: 814–831. doi:10.1093/plcell/koaa002

60. Ashikawa I, Hayashi N, Yamane H, Kanamori H, Wu J, Matsumoto T, et al. Two Adjacent Nucleotide-Binding Site–Leucine-Rich Repeat Class Genes Are Required to Confer Pikm-Specific Rice Blast Resistance. Genetics. 2008;180: 2267–2276. doi:10.1534/genetics.108.095034

61. Lee S-K, Song M-Y, Seo Y-S, Kim H-K, Ko S, Cao P-J, et al. Rice Pi5-Mediated Resistance to Magnaporthe oryzae Requires the Presence of Two Coiled-Coil–Nucleotide-Binding–Leucine-Rich Repeat Genes. Genetics. 2009;181: 1627–1638. doi:10.1534/genetics.108.099226

62. Narusaka M, Shirasu K, Noutoshi Y, Kubo Y, Shiraishi T, Iwabuchi M, et al. RRS1 and RPS4 provide a dual Resistance-gene system against fungal and bacterial pathogens. Plant J. 2009;60: 218–226. doi:10.1111/j.1365-313X.2009.03949.x

63. Okuyama Y, Kanzaki H, Abe A, Yoshida K, Tamiru M, Saitoh H, et al. A multifaceted genomics approach allows the isolation of the rice Pia-blast resistance gene consisting of two adjacent NBS-LRR protein genes. Plant J. 2011;66: 467–479. doi:10.1111/j.1365-313X.2011.04502.x

64. Białas A, Zess EK, De la Concepcion JC, Franceschetti M, Pennington HG, Yoshida K, et al. Lessons in Effector and NLR Biology of Plant-Microbe Systems. Mol Plant-Microbe Interactions. 2018;31: 34–45. doi:10.1094/MPMI-08-17-0196-FI

65. Césari S, Bernoux M, Moncuquet P, Kroj T, Dodds P. A novel conserved mechanism for plant NLR protein pairs: the 'integrated decoy' hypothesis. Front Plant Sci. 2014;5. doi:10.3389/fpls.2014.00606

66. Cesari S. Multiple strategies for pathogen perception by plant immune receptors. New Phytol. 2018;219: 17–24. doi:10.1111/nph.14877

67. Takagi H, Uemura A, Yaegashi H, Tamiru M, Abe A, Mitsuoka C, et al. MutMap-Gap: whole-genome resequencing of mutant F2 progeny bulk combined with de novo assembly of gap regions identifies the rice blast resistance gene Pii. New Phytol. 2013;200: 276–283. doi:10.1111/nph.12369

68. Cesari S, Thilliez G, Ribot C, Chalvon V, Michel C, Jauneau A, et al. The Rice Resistance Protein Pair RGA4/RGA5 Recognizes the Magnaporthe oryzae Effectors AVR-Pia and AVR1-CO39 by Direct Binding. Plant Cell. 2013;25: 1463–1481. doi:10.1105/tpc.112.107201

69. Kanzaki H, Yoshida K, Saitoh H, Fujisaki K, Hirabuchi A, Alaux L, et al. Arms race co-evolution of Magnaporthe oryzae AVR-Pik and rice Pik genes driven by their physical interactions. Plant J. 2012;72: 894–907. doi:10.1111/j.1365-313X.2012.05110.x

70. De la Concepcion JC, Franceschetti M, Maqbool A, Saitoh H, Terauchi R, Kamoun S, et al. Polymorphic residues in rice NLRs expand binding and response to effectors of the blast pathogen. Nat Plants. 2018;4: 576–585. doi:10.1038/s41477-018-0194-x

71. Białas A, Langner T, Harant A, Contreras MP, Stevenson CE, Lawson DM, et al. Two NLR immune receptors acquired high-affinity binding to a fungal effector through convergent evolution of their integrated domain. Monaghan J, Kleine-Vehn J, Delaux P-M, editors. eLife. 2021;10: e66961. doi:10.7554/eLife.66961

72. De la Concepcion JC, Maidment JHR, Longya A, Xiao G, Franceschetti M, Banfield MJ. The allelic rice immune receptor Pikh confers extended resistance to strains of the blast fungus through a single polymorphism in the effector binding interface. Birch P, editor. PLOS Pathog. 2021;17: e1009368. doi:10.1371/journal.ppat.1009368

73. Ortiz D, de Guillen K, Cesari S, Chalvon V, Gracy J, Padilla A, et al. Recognition of the Magnaporthe oryzae Effector AVR-Pia by the Decoy Domain of the Rice NLR Immune Receptor RGA5. Plant Cell. 2017;29: 156–168. doi:10.1105/tpc.16.00435

74. Guo L, Cesari S, de Guillen K, Chalvon V, Mammri L, Ma M, et al. Specific recognition of two MAX effectors by integrated HMA domains in plant immune receptors involves distinct binding surfaces. Proc Natl Acad Sci. 2018;115: 11637–11642. doi:10.1073/pnas.1810705115

75. Oikawa K, Fujisaki K, Shimizu M, Takeda T, Saitoh H, Hirabuchi A, et al. The blast pathogen effector AVR-Pik binds and stabilizes rice heavy metal-associated (HMA) proteins to co-opt their function in immunity. bioRxiv; 2020. p. 2020.12.01.406389. doi:10.1101/2020.12.01.406389

76. Fukuoka S, Saka N, Koga H, Ono K, Shimizu T, Ebana K, et al. Loss of Function of a Proline-Containing Protein Confers Durable Disease Resistance in Rice. Science. 2009;325: 998–1001. doi:10.1126/science.1175550

77. Maidment JHR, Franceschetti M, Maqbool A, Saitoh H, Jantasuriyarat C, Kamoun S, et al. Multiple variants of the fungal effector AVR-Pik bind the HMA domain of the rice protein OsHIPP19, providing a foundation to engineer plant defense. J Biol Chem. 2021;296. doi:10.1016/j.jbc.2021.100371

78. Fujisaki K, Abe Y, Kanzaki E, Ito K, Utsushi H, Saitoh H, et al. An unconventional NOI/RIN4 domain of a rice NLR protein binds host EXO70 protein to confer fungal immunity. bioRxiv; 2017. p. 239400. doi:10.1101/239400

79. Fujisaki K, Abe Y, Ito A, Saitoh H, Yoshida K, Kanzaki H, et al. Rice Exo70 interacts with a fungal effector, AVR-Pii, and is required for AVR-Pii-triggered immunity. Plant J. 2015;83: 875–887. doi:10.1111/tpj.12934

80. De la Concepcion JC, Franceschetti M, MacLean D, Terauchi R, Kamoun S, Banfield MJ. Protein engineering expands the effector recognition profile of a rice NLR immune receptor. Nürnberger T, Weigel D, Nürnberger T, editors. eLife. 2019;8: e47713. doi:10.7554/eLife.47713

81. Kourelis J, Marchal C, Kamoun S. NLR immune receptor-nanobody fusions confer plant disease resistance. bioRxiv; 2021. doi:10.1101/2021.10.24.465418

82. Liu Y, Zhang X, Yuan G, Wang D, Zheng Y, Ma M, et al. A designer rice NLR immune receptor confers resistance to the rice blast fungus carrying noncorresponding avirulence effectors. Proc Natl Acad Sci. 2021;118: e2110751118. doi:10.1073/pnas.2110751118

83. Cesari S, Xi Y, Declerck N, Chalvon V, Mammri L, Pugnière M, et al. New recognition specificity in a plant immune receptor by molecular engineering of its integrated domain. Nat Commun. 2022;13: 1524. doi:10.1038/s41467-022-29196-6

84. Marchal C, Michalopoulou VA, Zou Z, Cevik V, Sarris PF. Show me your ID: NLR immune receptors with integrated domains in plants. Essays Biochem. 2022; EBC20210084. doi:10.1042/EBC20210084

85. Maidment JH, Shimizu M, Vera S, Franceschetti M, Longya A, Stevenson CE, et al. Effector target-guided engineering of an integrated domain expands the disease resistance profile of a rice NLR immune receptor. bioRxiv; 2022. p. 2022.06.14.496076. doi:10.1101/2022.06.14.496076

86. Wang B, Ebbole DJ, Wang Z. The arms race between Magnaporthe oryzae and rice: Diversity and interaction of Avr and R genes. J Integr Agric. 2017;16: 2746–2760. doi:10.1016/S2095-3119(17)61746-5

87. Yuan B, Zhai C, Wang W, Zeng X, Xu X, Hu H, et al. The Pik-p resistance to Magnaporthe oryzae in rice is mediated by a pair of closely linked CC-NBS-LRR genes. Theor Appl Genet. 2011;122: 1017–1028. doi:10.1007/s00122-010-1506-3

88. Zhai C, Lin F, Dong Z, He X, Yuan B, Zeng X, et al. The isolation and characterization of Pik, a rice blast resistance gene which emerged after rice domestication. New Phytol. 2011;189: 321–334. doi:10.1111/j.1469-8137.2010.03462.x

89. Ashikawa I, Hayashi N, Abe F, Wu J, Matsumoto T. Characterization of the rice blast resistance gene Pik cloned from Kanto51. Mol Breed. 2012;30: 485–494. doi:10.1007/s11032-011-9638-y

90. Zhai C, Zhang Y, Yao N, Lin F, Liu Z, Dong Z, et al. Function and Interaction of the Coupled Genes Responsible for Pik-h Encoded Rice Blast Resistance. PLOS ONE. 2014;9: e98067. doi:10.1371/journal.pone.0098067

91. Chen J, Peng P, Tian J, He Y, Zhang L, Liu Z, et al. Pike, a rice blast resistance allele consisting of two adjacent NBS–LRR genes, was identified as a novel allele at the Pik locus. Mol Breed. 2015;35: 117. doi:10.1007/s11032-015-0305-6

92. Li J, Wang Q, Li C, Bi Y, Fu X, Wang R. Novel haplotypes and networks of AVR-Pik alleles in Magnaporthe oryzae. BMC Plant Biol. 2019;19: 204. doi:10.1186/s12870-019-1817-8

93. Takahashi A, Hayashi N, Miyao A, Hirochika H. Unique features of the rice blast resistance Pish locus revealed by large scale retrotransposon-tagging. BMC Plant Biol. 2010;10: 175. doi:10.1186/1471-2229-10-175

94. Zdrzałek R, Kamoun S, Terauchi R, Saitoh H, Banfield MJ. The rice NLR pair Pikp-1/Pikp-2 initiates cell death through receptor cooperation rather than negative regulation. PLOS ONE. 2020;15: e0238616. doi:10.1371/journal.pone.0238616

95. Simão FA, Waterhouse RM, Ioannidis P, Kriventseva EV, Zdobnov EM. BUSCO: assessing genome assembly and annotation completeness with single-copy orthologs. Bioinformatics. 2015;31: 3210–3212. doi:10.1093/bioinformatics/btv351

96. Dean RA, Talbot NJ, Ebbole DJ, Farman ML, Mitchell TK, Orbach MJ, et al. The genome sequence of the rice blast fungus Magnaporthe grisea. Nature. 2005;434: 980–986. doi:10.1038/nature03449

97. Bao J, Chen M, Zhong Z, Tang W, Lin L, Zhang X, et al. PacBio Sequencing Reveals Transposable Elements as a Key Contributor to Genomic Plasticity and Virulence Variation in Magnaporthe oryzae. Mol Plant. 2017;10: 1465–1468. doi:10.1016/j.molp.2017.08.008

98. Gómez Luciano LB, Tsai IJ, Chuma I, Tosa Y, Chen Y-H, Li J-Y, et al. Blast Fungal Genomes Show Frequent Chromosomal Changes, Gene Gains and Losses, and Effector Gene Turnover. Mol Biol Evol. 2019;36: 1148–1161. doi:10.1093/molbev/msz045

99. Win J, Harant A, Malmgren A, Langner T, Shrestha R-K, Latorre SM, et al. Large scale genome assemblies of Magnaporthe oryzae rice isolates from Italy. 2020 [cited 22 Mar 2022]. doi:10.5281/zenodo.4326823

100. Slater GSC, Birney E. Automated generation of heuristics for biological sequence comparison. BMC Bioinformatics. 2005;6: 31. doi:10.1186/1471-2105-6-31

101. Starnes JH, Thornbury DW, Novikova OS, Rehmeyer CJ, Farman ML. Telomere-Targeted Retrotransposons in the Rice Blast Fungus Magnaporthe oryzae: Agents of Telomere Instability. Genetics. 2012;191: 389–406. doi:10.1534/genetics.111.137950

102. Enright AJ, Van Dongen S, Ouzounis CA. An efficient algorithm for large-scale detection of protein families. Nucleic Acids Res. 2002;30: 1575–1584. doi:10.1093/nar/30.7.1575

103. Jumper J, Evans R, Pritzel A, Green T, Figurnov M, Ronneberger O, et al. Highly accurate protein structure prediction with AlphaFold. Nature. 2021;596: 583–589. doi:10.1038/s41586-021-03819-2

104. Zhang Y, Skolnick J. TM-align: a protein structure alignment algorithm based on the TM-score. Nucleic Acids Res. 2005;33: 2302–2309. doi:10.1093/nar/gki524

105. Xu J, Zhang Y. How significant is a protein structure similarity with TM-score = 0.5? Bioinformatics. 2010;26: 889–895. doi:10.1093/bioinformatics/btq066

106. Xue M, Yang J, Li Z, Hu S, Yao N, Dean RA, et al. Comparative Analysis of the Genomes of Two Field Isolates of the Rice Blast Fungus Magnaporthe oryzae. PLOS Genet. 2012;8: e1002869. doi:10.1371/journal.pgen.1002869

107. Longya A, Chaipanya C, Franceschetti M, Maidment JHR, Banfield MJ, Jantasuriyarat C. Gene Duplication and Mutation in the Emergence of a Novel Aggressive Allele of the AVR-Pik Effector in the Rice Blast Fungus. Mol Plant-Microbe Interactions. 2019;32: 740–749. doi:10.1094/MPMI-09-18-0245-R

108. Zhu K, Bao J, Zhang L, Yang X, Li Y, Zhu M, et al. Comparative analysis of the genome of the field isolate V86010 of the rice blast fungus Magnaporthe oryzae from Philippines. J Integr Agric. 2017;16: 2222–2230. doi:10.1016/S2095-3119(16)61607-6

109. Zhong Z, Norvienyeku J, Chen M, Bao J, Lin L, Chen L, et al. Directional Selection from Host Plants Is a Major Force Driving Host Specificity in Magnaporthe Species. Sci Rep. 2016;6: 25591. doi:10.1038/srep25591

110. Kim K-T, Ko J, Song H, Choi G, Kim H, Jeon J, et al. Evolution of the Genes Encoding Effector Candidates Within Multiple Pathotypes of Magnaporthe oryzae. Front Microbiol. 2019;10. doi:10.3389/fmicb.2019.02575

111. Varden FA, Saitoh H, Yoshino K, Franceschetti M, Kamoun S, Terauchi R, et al. Cross-reactivity of a rice NLR immune receptor to distinct effectors from the rice blast pathogen Magnaporthe oryzae provides partial disease resistance. J Biol Chem. 2019;294: 13006–13016. doi:10.1074/jbc.RA119.007730

112. Raffaele S, Farrer RA, Cano LM, Studholme DJ, MacLean D, Thines M, et al. Genome Evolution Following Host Jumps in the Irish Potato Famine Pathogen Lineage. Science. 2010;330: 1540–1543. doi:10.1126/science.1193070

113. Raffaele S, Kamoun S. Genome evolution in filamentous plant pathogens: why bigger can be better. Nat Rev Microbiol. 2012;10: 417–430. doi:10.1038/nrmicro2790

114. Dong S, Raffaele S, Kamoun S. The two-speed genomes of filamentous pathogens: waltz with plants. Curr Opin Genet Dev. 2015;35: 57–65. doi:10.1016/j.gde.2015.09.001

115. Deng Y, Zhai K, Xie Z, Yang D, Zhu X, Liu J, et al. Epigenetic regulation of antagonistic receptors confers rice blast resistance with yield balance. Science. 2017;355: 962–965. doi:10.1126/science.aai8898

116. Murakami J, Tosa Y, Kataoka T, Tomita R, Kawasaki J, Chuma I, et al. Analysis of Host Species Specificity of Magnaporthe grisea Toward Wheat Using a Genetic Cross Between Isolates from Wheat and Foxtail Millet. Phytopathology. 2000;90: 1060–1067. doi:10.1094/PHYTO.2000.90.10.1060

117. Lo C-C, Chain PSG. Rapid evaluation and quality control of next generation sequencing data with FaQCs. BMC Bioinformatics. 2014;15: 366. doi:10.1186/s12859-014-0366-2

118. Schmieder R, Edwards R. Quality control and preprocessing of metagenomic datasets. Bioinformatics. 2011;27: 863–864. doi:10.1093/bioinformatics/btr026

119. Kawahara Y, de la Bastide M, Hamilton JP, Kanamori H, McCombie WR, Ouyang S, et al. Improvement of the Oryza sativa Nipponbare reference genome using next generation sequence and optical map data. Rice. 2013;6: 4. doi:10.1186/1939-8433-6-4

120. Li H, Durbin R. Fast and accurate short read alignment with Burrows-Wheeler transform. Bioinformatics. 2009;25: 1754–1760. doi:10.1093/bioinformatics/btp324

121. Li H, Handsaker B, Wysoker A, Fennell T, Ruan J, Homer N, et al. The Sequence Alignment/Map format and SAMtools. Bioinformatics. 2009;25: 2078–2079. doi:10.1093/bioinformatics/btp352

122. McKenna A, Hanna M, Banks E, Sivachenko A, Cibulskis K, Kernytsky A, et al. The Genome Analysis Toolkit: A MapReduce framework for analyzing next-generation DNA sequencing data. Genome Res. 2010;20: 1297–1303. doi:10.1101/gr.107524.110

123. Li H. A statistical framework for SNP calling, mutation discovery, association mapping and population genetical parameter estimation from sequencing data. Bioinformatics. 2011;27: 2987–2993. doi:10.1093/bioinformatics/btr509

124. Fragoso CA, Heffelfinger C, Zhao H, Dellaporta SL. Imputing Genotypes in Biallelic Populations from Low-Coverage Sequence Data. Genetics. 2016;202: 487–495. doi:10.1534/genetics.115.182071

125. De Coster W, D'Hert S, Schultz DT, Cruts M, Van Broeckhoven C. NanoPack: visualizing and processing long-read sequencing data. Bioinformatics. 2018;34: 2666–2669. doi:10.1093/bioinformatics/bty149

126. Chen Y, Nie F, Xie S-Q, Zheng Y-F, Dai Q, Bray T, et al. Efficient assembly of nanopore reads via highly accurate and intact error correction. Nat Commun. 2021;12: 60. doi:10.1038/s41467-020-20236-7

127. Vaser R, Sović I, Nagarajan N, Šikić M. Fast and accurate de novo genome assembly from long uncorrected reads. Genome Res. 2017;27: 737–746. doi:10.1101/gr.214270.116

128. Kundu R, Casey J, Sung W-K. HyPo: Super Fast & Accurate Polisher for Long Read Genome Assemblies. bioRxiv; 2019 Dec. doi:10.1101/2019.12.19.882506

129. Roach MJ, Schmidt SA, Borneman AR. Purge Haplotigs: allelic contig reassignment for third-gen diploid genome assemblies. BMC Bioinformatics. 2018;19: 460. doi:10.1186/s12859-018-2485-7

130. Alonge M, Lebeigle L, Kirsche M, Aganezov S, Wang X, Lippman ZB, et al. Automated assembly scaffolding elevates a new tomato system for high-throughput genome editing. bioRxiv; 2021 Nov. doi:10.1101/2021.11.18.469135

131. Miki D, Shimamoto K. Simple RNAi Vectors for Stable and Transient Suppression of Gene Function in Rice. Plant Cell Physiol. 2004;45: 490–495. doi:10.1093/pcp/pch048

132. Hiei Y, Ohta S, Komari T, Kumashiro T. Efficient transformation of rice (Oryza sativa L.) mediated by Agrobacterium and sequence analysis of the boundaries of the T-DNA. Plant J. 1994;6: 271–282. doi:10.1046/j.1365-313X.1994.6020271.x

133. Katoh K, Standley DM. MAFFT Multiple Sequence Alignment Software Version 7: Improvements in Performance and Usability. Mol Biol Evol. 2013;30: 772–780. doi:10.1093/molbev/mst010

134. Minh BQ, Schmidt HA, Chernomor O, Schrempf D, Woodhams MD, von Haeseler A, et al. IQ-TREE 2: New Models and Efficient Methods for Phylogenetic Inference in the Genomic Era. Mol Biol Evol. 2020;37: 1530–1534. doi:10.1093/molbev/msaa015

135. Hoang DT, Chernomor O, von Haeseler A, Minh BQ, Vinh LS. UFBoot2: Improving the Ultrafast Bootstrap Approximation. Mol Biol Evol. 2018;35: 518–522. doi:10.1093/molbev/msx281

136. Kalyaanamoorthy S, Minh BQ, Wong TKF, von Haeseler A, Jermiin LS. ModelFinder: fast model selection for accurate phylogenetic estimates. Nat Methods. 2017;14: 587–589. doi:10.1038/nmeth.4285

137. Xiao C-L, Chen Y, Xie S-Q, Chen K-N, Wang Y, Han Y, et al. MECAT: fast mapping, error correction, and de novo assembly for single-molecule sequencing reads. Nat Methods. 2017;14: 1072–1074. doi:10.1038/nmeth.4432

138. Stanke M, Diekhans M, Baertsch R, Haussler D. Using native and syntenically mapped cDNA alignments to improve de novo gene finding. Bioinformatics. 2008;24: 637–644. doi:10.1093/bioinformatics/btn013

139. Cabanettes F, Klopp C. D-GENIES: dot plot large genomes in an interactive, efficient and simple way. PeerJ. 2018;6: e4958. doi:10.7717/peerj.4958

140. Quinlan AR, Hall IM. BEDTools: a flexible suite of utilities for comparing genomic features. Bioinformatics. 2010;26: 841–842. doi:10.1093/bioinformatics/btq033

141. Li H. Minimap2: pairwise alignment for nucleotide sequences. Birol I, editor. Bioinformatics. 2018;34: 3094–3100. doi:10.1093/bioinformatics/bty191

142. Wu Y, Bhat PR, Close TJ, Lonardi S. Efficient and Accurate Construction of Genetic Linkage Maps from the Minimum Spanning Tree of a Graph. PLOS Genet. 2008;4: e1000212. doi:10.1371/journal.pgen.1000212

143. Sugihara Y, Darkwa K, Yaegashi H, Natsume S, Shimizu M, Abe A, et al. Genome analyses reveal the hybrid origin of the staple crop white Guinea yam (Dioscorea rotundata). Proc Natl Acad Sci. 2020;117: 31987–31992. doi:10.1073/pnas.2015830117

144. Ou S, Su W, Liao Y, Chougule K, Agda JRA, Hellinga AJ, et al. Benchmarking transposable element annotation methods for creation of a streamlined, comprehensive pipeline. Genome Biol. 2019;20: 275. doi:10.1186/s13059-019-1905-y

145. Iwata H, Gotoh O. Benchmarking spliced alignment programs including Spaln2, an extended version of Spaln that incorporates additional species-specific features. Nucleic Acids Res. 2012;40: e161. doi:10.1093/nar/gks708

146. Endelman JB. Ridge Regression and Other Kernels for Genomic Selection with R Package rrBLUP. Plant Genome. 2011;4. doi:10.3835/plantgenome2011.08.0024

147. Kim D, Langmead B, Salzberg SL. HISAT: a fast spliced aligner with low memory requirements. Nat Methods. 2015;12: 357–360. doi:10.1038/nmeth.3317

148. Kovaka S, Zimin AV, Pertea GM, Razaghi R, Salzberg SL, Pertea M. Transcriptome assembly from long-read RNA-seq alignments with StringTie2. Genome Biol. 2019;20: 278. doi:10.1186/s13059-019-1910-1

149. Sweigard J, Chumley F, Carroll A, Farrall L, Valent B. A series of vectors for fungal transformation. Fungal Genet Rep. 1997;44: 52–53. doi:10.4148/1941-4765.1287

150. Needleman SB, Wunsch CD. A general method applicable to the search for similarities in the amino acid sequence of two proteins. J Mol Biol. 1970;48: 443–453. doi:10.1016/0022-2836(70)90057-4

151. Camacho C, Coulouris G, Avagyan V, Ma N, Papadopoulos J, Bealer K, et al. BLAST+: architecture and applications. BMC Bioinformatics. 2009;10: 421. doi:10.1186/1471-2105-10-421

152. Teufel F, Almagro Armenteros JJ, Johansen AR, Gíslason MH, Pihl SI, Tsirigos KD, et al. SignalP 6.0 predicts all five types of signal peptides using protein language models. Nat Biotechnol. 2022; 1–3. doi:10.1038/s41587-021-01156-3

153. Pettersen EF, Goddard TD, Huang CC, Meng EC, Couch GS, Croll TI, et al. UCSF ChimeraX: Structure visualization for researchers, educators, and developers. Protein Sci. 2021;30: 70–82. doi:10.1002/pro.3943

154. Van der Hoorn RAL, Laurent F, Roth R, De Wit PJGM. Agroinfiltration Is a Versatile Tool That Facilitates Comparative Analyses of Avr9/Cf-9-Induced and Avr4/Cf-4-Induced Necrosis. Mol Plant-Microbe Interactions. 2000;13: 439–446. doi:10.1094/MPMI.2000.13.4.439

155. Kourelis J, Malik S, Mattinson O, Krauter S, Kahlon PS, Paulus JK, et al. Evolution of a guarded decoy protease and its receptor in solanaceous plants. Nat Commun. 2020;11: 4393. doi:10.1038/s41467-020-18069-5

156. Césari S, Kanzaki H, Fujiwara T, Bernoux M, Chalvon V, Kawano Y, et al. The NB-LRR proteins RGA4 and RGA5 interact functionally and physically to confer disease resistance. EMBO J. 2014;33: 1941–1959. doi:10.15252/embj.201487923

157. De la Concepcion JC, Vega Benjumea J, Bialas A, Terauchi R, Kamoun S, Banfield MJ. Functional diversification gave rise to allelic specialization in a rice NLR immune receptor pair. Zhou J-M, Kleine-Vehn J, Zhou J-M, Chae E, editors. eLife. 2021;10: e71662. doi:10.7554/eLife.71662